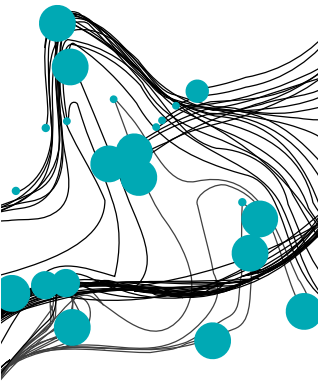

RAM ROBOTICS AND MECHATRONICS

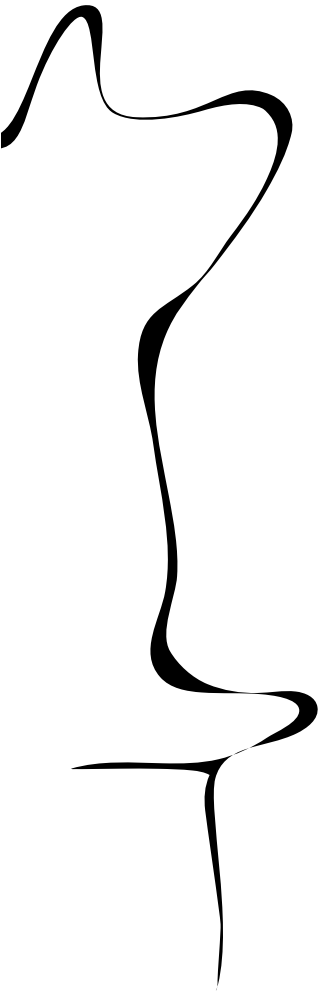

DEVELOPMENT OF A 3D-PRINTED ANGLE SENSOR FOR FEEDBACK IN SOFT ROBOTIC APPLICATIONS

Adrita Bima Adi

MSC ASSIGNMENT

Committee:
prof. dr. ir. G.J.M. Krijnen
G.J.W. Wolterink, MSc
dr. ir. M. Abayazid
prof. dr. ir. P.H. Veltink

February, 2021

007RaM2021
Robotics and Mechatronics
EEMCS
University of Twente
P.O. Box 217
7500 AE Enschede
The Netherlands

UNIVERSITY OF TWENTE. | TECHMED CENTRE UNIVERSITY OF TWENTE. | DIGITAL SOCIETY INSTITUTE

Abstract

This thesis describes the early development of 3D printed resistive length sensors to measure bending movement in soft endoscope. The sensors are printed using fused deposition modeling (FDM) 3D printer with multi-material printing ability. Conductive and non-conductive thermoplastic polyurethane (TPU) are used as the materials of the sensors. The sensors are embedded inside the soft endoscope module during the fabrication of the module.

Vertical module elongation test is done to characterize the resistance change caused by the elongation of the sensors inside the module. Different elongation between the chambers results in bending movement. The bending and orientation angle of the module are converted from the length of each sensor using constant curvature kinematics. The data calculated from the length sensors are compared to electromagnetic tracker to validate the usability of the sensors.

The results show that the approach of using 3D printed resistive length sensors to measure bending movement is not the best approach. The non-linearity of the material and its rate dependant hysteresis are big problems in length sensors. Embedding the sensors, although it helps to utilize unused space inside the module, is affecting the strain perceived by the sensors. The measured strain by the sensors is not only the desired elongation but also strain caused by chambers inflation.

Contents

List of Figures

List of Tables

Chapter 1

INTRODUCTION

1.1 BACKGROUND

Soft robotics is a growing field of research about using compliant materials to implement robotic systems [11]. The implementation is often inspired by nature and might give a solution to a problem that cannot be addressed by a conventional robot built from rigid bodies. One possible application of soft robotics is in the medical field. The compliance characteristic is advantageous to minimize the risk of damaging human body tissues. In this research, the application is soft endoscope.

An endoscope is a tube-shaped optical device used to look inside the human body. This device is usually used to visually examine human internal organs or assist in surgery. The endoscope in this research is made from a bio-compatible material (silicone elastomer) and actuated by giving air pressure into the pneumatic chambers [17]. The endoscope consists of several endoscope modules. These endoscope modules are able to bend separately to achieve a specific shape. The bending motion of the endoscope module is the main interest in this research.

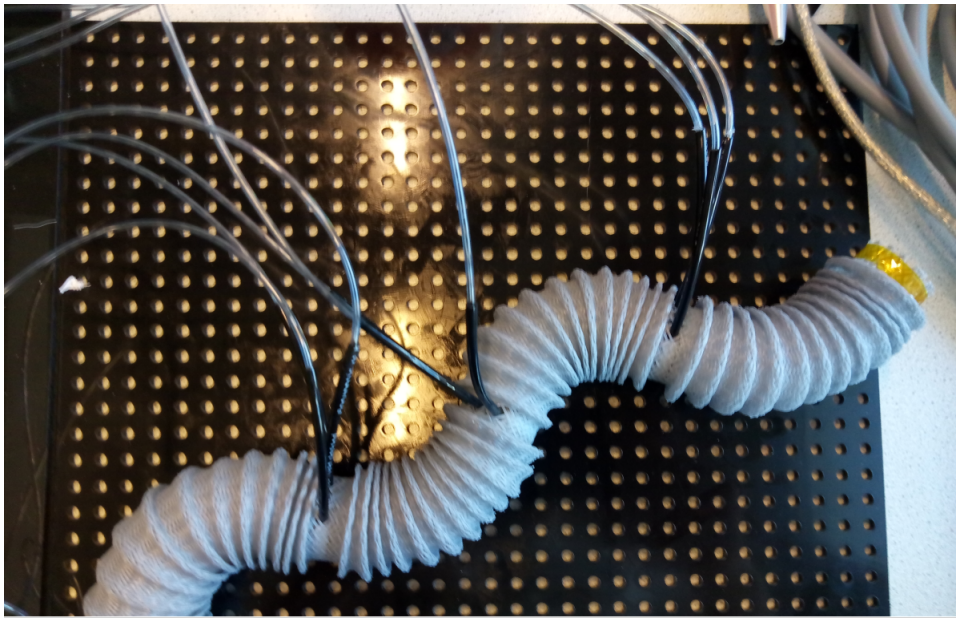

Figure 1.1: Soft endoscope with four modules connected together [15].

One of the major problems of the soft robotics is to gauge its position to be able to control its motion [1]. A sensor is needed to enable a closed-loop control resulting in controllable behavior. The sensor can be an external or an internal sensor. An external sensor is a sensor that needs additional external device to capture the intended data (e.g. camera, magnetic sensor). An internal sensor is a sensor placed inside the robot and can provide the intended data without additional external device. Taking into consideration that the soft endoscope is going inside the human body and might use magnetic resonance imaging (MRI) as a complementary device, it is in our best interest to build an internal sensor. Embedding the sensor directly into the endoscope module is more beneficial because it does not require line of sight, does not add to the size of the module, and it utilizes unused space inside the module.

As a conventional sensor may not be a good fit for controlling the soft endoscope module; therefore, a customizable sensor is needed. A conventional sensor tends to have a standard shape that may not be able to be used together with the endoscope module. A customizable sensor can be made using 3D printing method [31]. This method is a form of rapid prototyping. There are many fabrication methods and materials for 3D printing. The most common used method in 3D printing is fused deposition modeling (FDM). FDM works by extruding a filament layer-by-layer to make a solid structure. The development and fabrication of the sensor can be done faster and cheaper than a conventional sensor. Another benefit of 3D printing is that it allows for the creation of specific geometric shape to meet the system requirements.

Considering the fact that the sensor is going to be embedded inside the soft endoscope module, it is beneficial to also use flexible materials. A filament made from thermoplastic polyurethane (TPU) has elastic properties. There is a type of TPU that contains graphitized carbon fill to make it conductive. The commercial name for this conductive TPU filament is ETPU [29]. The conductivity and flexibility of ETPU benefits sensor fabrication in soft robotics application. Printing the sensor also allows further development if in the future it is already possible to print the whole endoscope. Currently, all soft robotics implementations and their sensors are made separately and later assembled together. A 3D-printed sensor might still be relevant from this point forward, seeing that multi-material 3D printing is on the rise.

1.2 RESEARCH PURPOSE

The main research question is “How to utilize FDM 3D printing methods to develop a bending sensor for feedback in soft endoscope application?”.

The purpose of this research can be derived from the research question. It is to make a sensor that is able to measure both bending angle and orientation of the endoscope module using FDM 3D printing especially with ETPU as its main material.

1.3 RELATED WORKS

The research on the endoscope module was initially started by Wildan Gifari [17]. However, the specific endoscope module that was used in this research is based on the latest iteration by Jornt Lageveen [15]. It is a STIFF-FLOP surgical manipulator with three circle chambers without inner sheeting. The module is discussed further in the next chapter.

Some previous internal sensor implementations in the soft robotics can be classified into three big groups: strain gauge, Hall sensor, and optoelectronic [28]. A strain gauge is a type of sensor that changes its resistance or capacitance depending on the applied force. Its application varies from using ionic liquid [20], conductive fiber [27], and conductive filament [10]. The second possible implementation is the Hall sensor. Hall sensors measure the magnitude of magnetic field. The usual practice to implement this is by placing the sensor on one end of the bending module and placing the magnet on the opposite end [16]. As the module bends, the distance between the magnet and the sensor also changes, hence the measured magnetic field also changes [18]. The third option is optoelectronic. Optoelectronic is the implementation of electronic device to modulate light [32]. An optical fiber is used to propagate light, a photodiode is used to measure the intensity on the other side of the light source. The light intensity varies due to attenuation caused by the optical fiber bending, this phenomenon is used as the basic principle of this kind of sensor. All of these sensors are feasible solutions to fill the sensing part in the soft endoscope module and going to be discussed further in the next chapter regarding their capabilities to fulfill the system requirements.

The methods mentioned above are for the general soft robotics. One previous work to specifically measure bending and orientation angle of a STIFF-FLOP module was done by using fiber-optics [23]. The aim of the mentioned work is to characterize the main parameters of the fiber-optics as stretch sensors and then to integrate the stretch sensors into the STIFF-FLOP module for pose measurement. This previous work is the basis of this research.

1.4 REPORT OUTLINE

This report is presented in seven chapters. The first chapter is a brief introduction to the background and purpose of the research. The second chapter is the analysis of the requirements. The third chapter discusses the sensor design followed by the fabrication of the sensors and the assembly process with the endoscope module in the fourth chapter. In the fifth chapter, the detailed experiment setup to evaluate the sensor is discussed. The experiment results are presented and further discussed in the sixth chapter. The last chapter are the conclusions of the current research and possible recommendations for the next research.

Chapter 2

ANALYSIS

2.1 STIFF-FLOP MODULE

As mentioned before, the module that was used in this research is a STIFF-FLOP module. STIFF-FLOP is an abbreviation of **STIFF**ness controllable **F**lexible and **L**earn-able manipulator for surgical **OP**erations. There are three pneumatic chambers inside the module and it has a hollow part at the center of each module for transport of surgical and optical devices. The pressure makes the pneumatic chamber elongates and different elongation between the chambers results in bending [17]. The dimension of the STIFF-FLOP module in this research is shown in Figure 2.2.

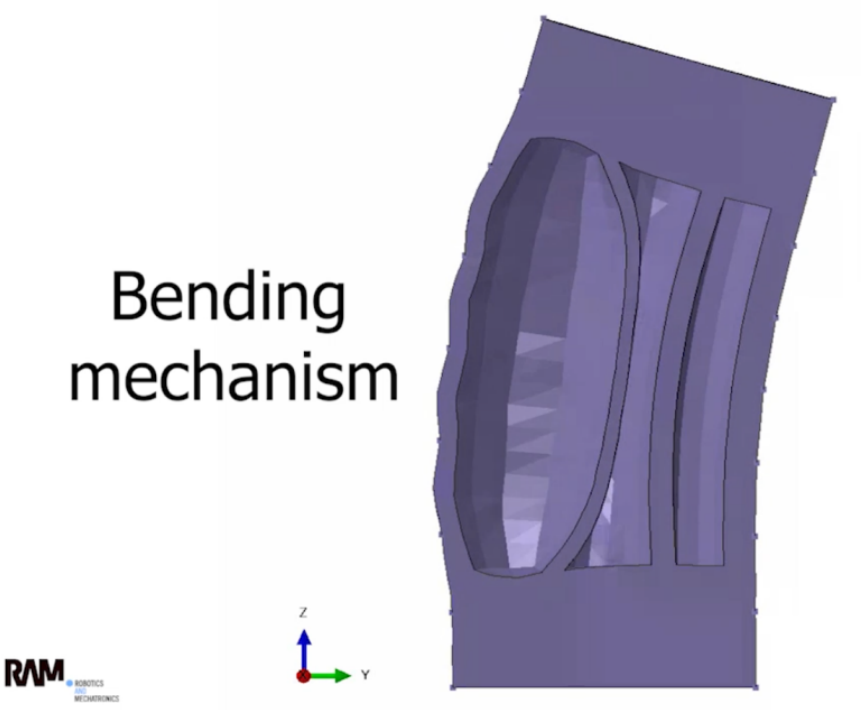

Figure 2.1: The expansion of the chamber resulting in the bending motion of the STIFF-FLOP module [17].

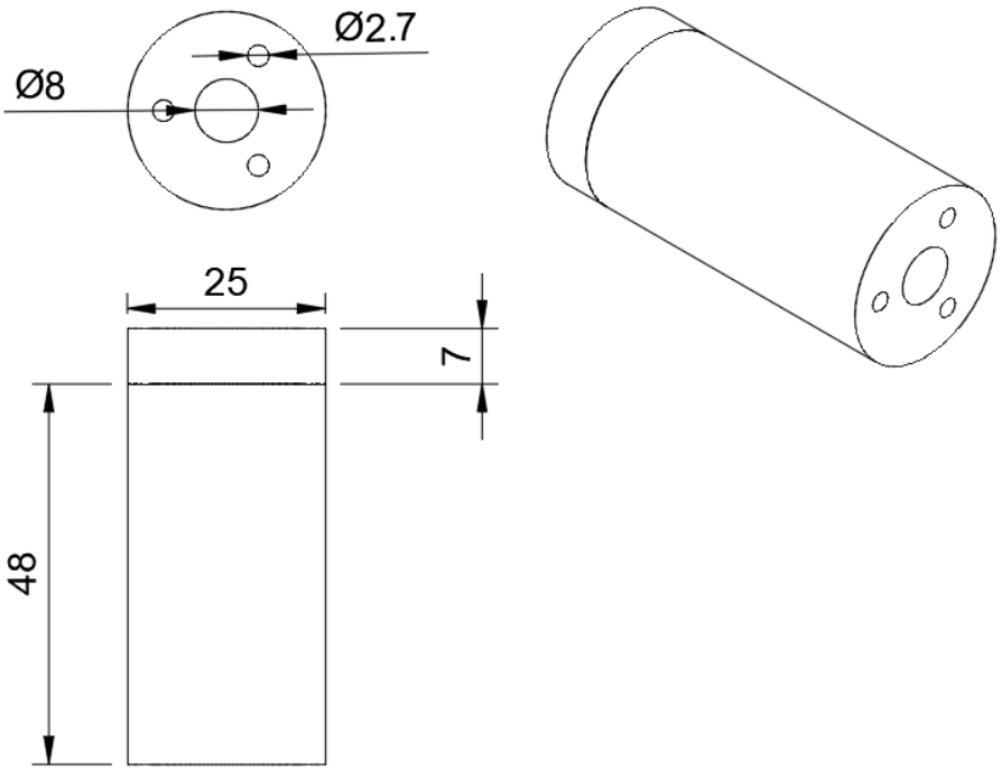

Figure 2.2: The drawing with dimension of the STIFF-FLOP module in this research (in mm).

2.2 REQUIREMENTS

This section explains the details of the expected requirements of the bending sensor in this research. According to [21], there are three basic requirements for sensing part in soft robotics:

- The sensor should be compliant enough; therefore, it does not affect the properties of the soft endoscope module.
- The sensor should have enough durability as one of its characteristics, hence it is able to withstand many deformation (stretch) cycles.
- The sensor should not damage the soft parts of the system.

The design of the sensor, as a part of the whole system, should also consider other elements it interacts with (e.g. available space, elasticity of the module). This causes some limitations to emerge. Using these limitations, the requirements of the sensor can be further defined as: application requirements, actuator requirements, and sensor requirements.

APPLICATION REQUIREMENTS

The application requirements consider the dimension of the whole system and how the whole system is going to work. As stated in Chapter 1, the soft endoscope

consists of multiple modules that can bend independently. Each module has three pneumatic chambers as the actuators and hollow center part for other devices. Taking into account all of the mentioned system characteristics, the application requirements are:

- **The sensor can at least measure 3 DOF.**
  There are three chambers that can be activated separately, hence at least there are three bending directions in the 3D space. The bending direction includes the amount of bending angle and also the bending orientation of the module. Combination of two or more activated chamber might result in other bending directions [17]. The sensor should also be able to capture these three directions.
- **Sensor development in multi modules setting.**
  In this research, the sensor is only applied in one endoscope module but in the future the modules are going to be controlled together. Hence, the method to measure the bending should also take this further development into account.
- **The sensor can be embedded into the module.**
  As mentioned before in Chapter 1, an embedded sensor is more favorable for this application. The endoscope is going inside the human body, consequently a big sensor or sensor requiring line of sight will not be ideal. The sensor should be simple enough to be installed and used. Its implementation should not make the usage of the endoscope more complicated.
- **The sensor setup does not interfere with the hollow center part of the module.**
  An embedded sensor should consider the available space inside the module and also the shape of the module. The hollow center part of the module is going to be filled with other optical and medical devices, thus leaving it empty is one of the requirements of the sensor setup. The setup of the sensor should not only leave the center part empty but also not interfere with the movement of the center part. Therefore, the dimension of the sensor should not exceed the remaining space of the module.
- **The electrical connection of the sensor should use as few as wires as possible.**
  The remaining space inside the module is pretty small and more wires inside the module means a lot more wires in multi modules setting. Although the soft endoscope is still in its early development, it is important to consider the electrical connection early because it is going to add up with increasing amount of endoscope segments. The wiring should not hinder the movement of the endoscope module.

ACTUATOR REQUIREMENTS

The next requirement type is actuator requirements. Actuator requirements are some sensor characteristic that need to be fulfilled in regard to its implementation effect to the characteristic of the pneumatic chamber of the soft endoscope. The requirements are closely related to how the actuators behave:

- **The sensor should not significantly reduce the amount of bending.** The sensor implementation inside the soft endoscope module has high possibility to change the compliance of the module. It might add more stiffness to the module. Stiffer modules have the potential to bend less. The implementation of the sensor should also not deter the actuation method using air pressure. The target is to see no more than 50% bending reduction.
- **The sensor should not significantly change the amount of pressure needed to bend the endoscope module.** The shape of the sensor or the means to measure the bending might affect the amount of pressure going inside the pneumatic chamber. There is a limit to amount of pressure that can be withstood by the module, hence it is necessary to consider the effect of the sensor to the pressure inside the actuator. The maximum amount of pressure that can be withstood by the STIFF-FLOP module is 0.55 bar. The target in this research is to be able to reach at least 0.4 bar where the change of bending angle is still pretty significant [15].

SENSOR REQUIREMENTS

The last one is the sensor requirements themselves. The sensor requirements are some sensing and manufacturing parameters that are needed to be satisfied by the sensor:

- **The sensor should have been able to be made using 3D printer.** One of the main focuses in this research is 3D printing method and its capability of faster prototyping and manufacturing. It is best if the whole part of the sensor can be manufactured using 3D printing method. The preferred 3D printing method in this research is FDM with ETPU as the main material.
- **The sensor should have acceptable resolution and error.** Resolution is the smallest change the sensor can detect. Referring to [17], a slight change (increment of 0.05 bar) to the applied pressure results in 5 degrees to 20 degrees change of bending angle depending on the current bending angle. A sensor that is able to measure 5 degrees change is presumably good enough. The maximum error of bending angle on [23] is 13%. Referring to this, the target for maximum error in this research is no more than 20%.
- **The sensor should only sensitive to the bending movement.** Seeing the environment where the sensor is going to be used, there might be some effect from outside the system. The sensor must have some resistance to the environment effect, such as temperature from the human body or magnetic field from the MRI machine.

All of the requirements can be summarized and prioritized using MoSCoW method. This method is a form of prioritization to focus the most important requirements first.

Table 2.1: Priority of the requirements with MoSCoW method.

Mo (Must-haves)	· Can be made using 3D printer. · Can measure 3 DOF.
S (Should-haves)	· Not significantly reduce the amount of bending. · Acceptable resolution and error. · Can be embedded.
Co (Could-haves)	· Multi modules setting. · Not significantly change the amount of pressure. · Not interfere with the hollow center part.
W (Won't - or Would-haves)	· Use as few as wires as possible. · Only sensitive to the bending.

2.3 SENSOR SELECTION

This section describes the choice of the sensor type. One of the purposes of this research is to build a sensor using 3D printing method; therefore, this is going to be the first consideration to choose what kind of sensor is going to be implemented.

Using thermoplastic with magnetic filler particles, a polymer bonded permanent magnet can be fabricated. It is also achievable to make different shapes of magnet to generate a specific stray field [12]. As stated before, the solution to measure the bending using magnet and Hall sensor is by placing the magnet at one end of the elastomer and placing the Hall sensor at the opposite end. When the elastomer bends, the magnetic flux will change. The previous implementation [16] [18] still used a commercial Hall sensor IC and magnet. Using 3D printer to manufacture magnet and Hall sensor is an interesting idea; however, this solution has conflicting things with the requirements. The first limitation is the incompatibility of the solution with the future application. The soft endoscope is going to be used with MRI machine, thus using magnet as a sensor is not possible. The second limitation is the material, the most common used material to manufacture a 3D-printed magnet is NdFeB and this material is outside the scope of this research. There is still no working 3D-printed Hall sensor [4], thus this solution still requires a commercial Hall sensor.

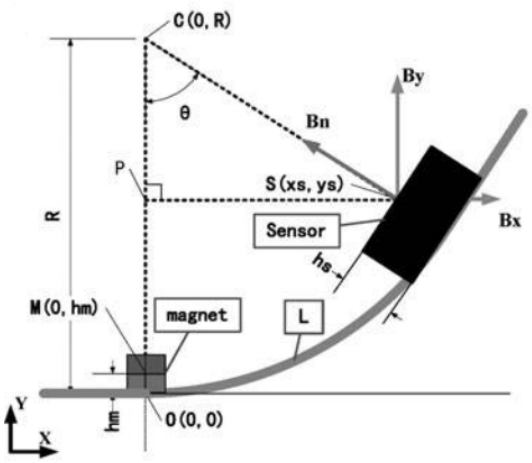

Figure 2.3: The bending model between the magnet and the Hall sensor [16].

Manufacturing optical element using 3D printer is already achievable. Light pipe is one of the possibilities [19] [30]. It is a structure that has the ability to transmit light in a similar manner to optical fiber, the light is reflecting as it travels the pipe. This is still an early implementation and the light transmission is limited by the pipe length and curvature. Beside the aforementioned limitations, the material used to make the light pipe is a rigid material named VeroClear. It is not desirable to embed rigid material inside the soft endoscope module. Consequently, the optoelectronic solution still requires commercial fiber-optics to be implemented.

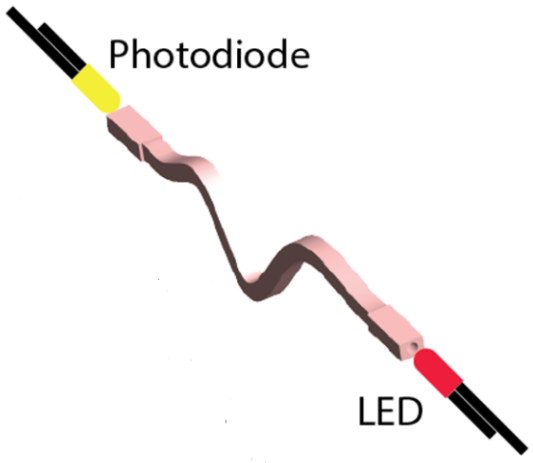

Figure 2.4: The illustration of how to measure curvature using light intensity [32].

A strain gauge is a type of sensor that has often been made using 3D printing method [3] [7] [10]. This kind of sensor can be made wholly using a 3D printer; thus, it fits the purpose of this research to utilize FDM method and conductive filament to manufacture a sensor. Compared to the other two solutions, a strain gauge can be made using elastic filament and is able to work inside magnetic field to some extent.

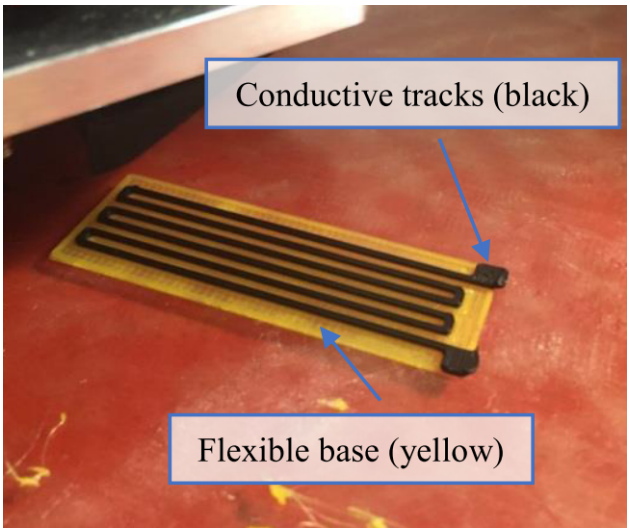

Figure 2.5: A 3D printed flexible strain sensor [10].

There are two types of strain gauge, resistive and capacitive. Both of them can be manufactured using 3D printing method. The resistive strain gauge can be made only from the conductive filament. On the other hand, the capacitive strain gauge needs another elastic filament as a dielectric material. There is no conclusive document that states which one is better between the capacitive and the resistive strain gauge. According to [25], the resistive type has higher gauge factor that translates to better strain detection. It is easier and faster to be manufactured. On the other hand, the capacitive sensor has better linearity and repeatability. However, the performance of a 3D-printed sensor is heavily affected by the materials, geometry, and printing direction. One advantage of the resistive strain gauge is the straightforward measurement. It is typically simpler to implement resistance measurement in a mechatronic system.

The module is bending because of the different elongation between the chambers. Based on how the module operates, the most straightforward solution to measure 3 DOF bending is by assembling at least three parallel strain gauges to measure each chamber elongation [23]. The combination of the sensors results in 3D sensing of the module, both bending angle (θ) and orientation (ϕ). The design approach of the sensor can be seen below.

θ, ϕ	⇔ Kinematics Model	length	⇔ Resistance Model	resistance	⇔ Electrical Model	voltage

Figure 2.6: The design approach of the sensor.

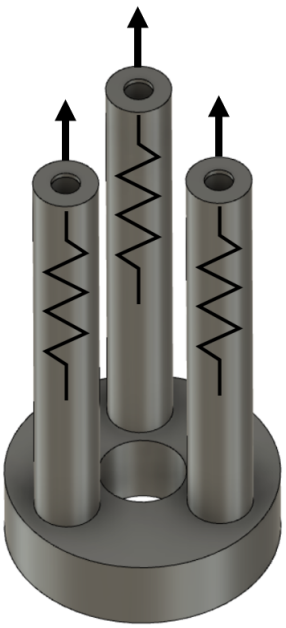

Figure 2.7: An illustration of how three parallel strain gauges measuring each chamber elongation.

2.4 CONCLUSION

The system requirements are introduced and prioritized. The sensors should be compliant, have enough durability, should not damage the soft parts of the system, can be made entirely using 3D printer, and can measure 3 DOF. The type of sensor that meets the top priorities of these requirements is strain gauge. The other two types of sensor, Hall sensor and optoelectronic, still need commercial components and cannot be fully printed. There are two types of strain gauge, resistive and capacitive. Resistive strain gauge is selected because of the more straightforward measurement.

The bending movement of the module is the result of different elongation between the chambers, therefore; the bending movement can also be measured by measuring each chamber elongation. The most direct approach is by assembling three parallel strain gauges to measure each chamber elongation. After the selection of the type of the sensor, the design approach is introduced. The kinematics model is the model that explains how the bending and orientation angle are connected to the length of the sensor. The resistance model defines how the length change of the sensor affecting its resistance. The electrical model demonstrates how to measure the resistance change as a voltage change. These models are explained further in the next chapter.

Chapter 3

DESIGN

3.1 SENSOR PLACEMENT

As mentioned in Chapter 2, the chosen measurement approach is by using three parallel strain gauges to measure the bending and orientation angle. This section discusses several ideas about where to place the sensors. There are three main ideas:

AROUND THE CHAMBERS

The general idea of this sensor placement is to improve the sensing ability of the sensor by placing it directly around the moving element, the chambers. The added value of this idea is also to help restricting the radial expansion of the chamber while improving the longitudinal expansion. The strain gauge shape idea for this kind of placement is a spiral. This placement idea and the spiral shape of the strain gauge were already tried to be implemented however the result was not satisfying. It was pretty hard to achieve a spiral shape with the currently available FDM printer. By placing the sensors around the chambers, the sensor were not embedded well inside the silicone module. The implementation can be seen on Appendix A.

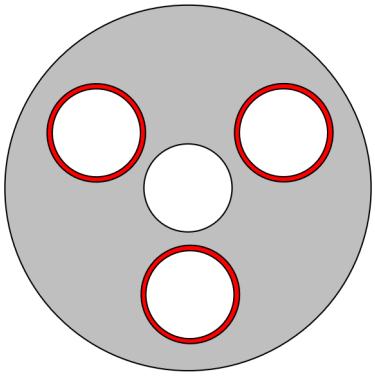

Figure 3.1: Illustration of sensors placement around the chamber (cross section view).

BETWEEN THE CHAMBERS

The purpose of this idea is to utilize unused space between the chambers. The sensor is not directly measuring the chamber elongation as the first idea. The sensors might

be slipping inside the silicone module while it moves because of different material surface roughness; therefore, the shape of the sensors must support better grip on the silicone.

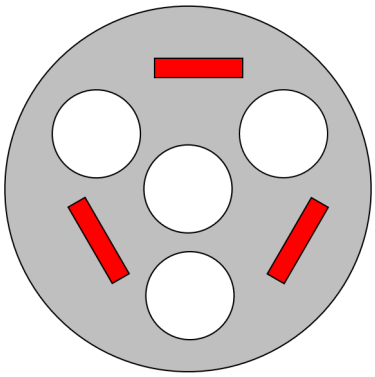

Figure 3.2: Illustration of sensors placement between the chambers (cross section view).

OUTSIDE THE MODULE

By placing the sensors outside the module, the direct measurement of the chamber elongation becomes possible again. It can be placed on the silicone module using adhesive or on the outer sheeting of the module. However, the sensors need to be very thin to be able to stick on the silicone module. The sensor produced using currently available FDM printer cannot withstand many stretch cycle if it is too thin. As for the placement on the outer sheeting, it was pretty hard to design a shape that can be stuck on the surface of the sheeting.

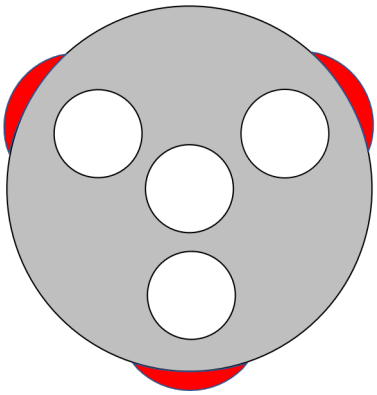

Figure 3.3: Illustration of sensors placement outside the module (cross section view).

Using currently available method, placing the sensors between the chambers is the most feasible solution. The first idea was already tried but the result was not good enough as stated above. The third idea was failed during the sensor fabrication process; therefore, it was not necessary to continue to module fabrication to see that the third idea is also not good enough.

3.2 SENSOR SHAPE DESIGN

A usual strain gauge has active grid section. Active grid section is where the strain gauge is sensitive to its length change [26]. Because the sensors should be able to measure the chamber elongation, the active grid section on the printed sensors should be parallel to the elongation direction of the chambers.

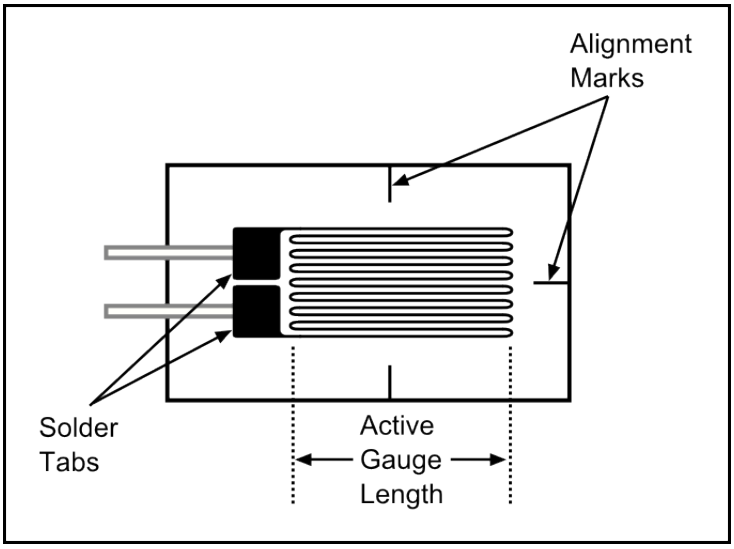

Figure 3.4: Sketch of commercial strain gauge [26].

As indicated earlier, the shape of the strain gauge needs to improve its grip on the silicone. The strain gauge will not be able to sense the elongation if it slips inside the silicone module because it will stay in its position while the silicone module elongates. A simple shape modification on the linear active grid section might help with the grip. A wavy shape on the active grid section is proposed to have "rougher" surface and bigger contact area between the sensor and the silicone. The proposed design is presented in Figure 3.5

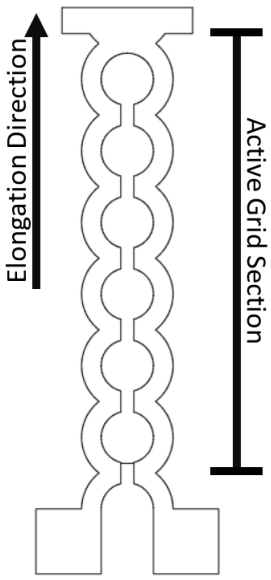

Figure 3.5: Proposed design of the sensor.

A commercial strain gauge usually has more than one zigzag cycle of the conductive material. However, due to limited space between the chambers and printer resolution, only one zigzag cycle is able to be made on the sensor. The top end of the sensor also has bigger area with sharp corner to help the sensor to hook the sensor with the silicone module. The component and exact dimension of the sensor are presented in the next chapter.

3.3 KINEMATICS MODEL

The kinematics model of this endoscope adopts the constant curvature continuum robots modeling. This model provides the means to measure bending and orientation angle by knowing the arc length of the robot [13]. The arc length of the robot in this experiment is measured by the length of the printed strain gauges. This kinematics model has an assumption that no external forces applied to the module and the module bends only because of the pressure inside the chambers.

The arc length (S) is the length combination of the three strain gauges (s_1, s_2, s_3). The bending orientation (ϕ) is the module orientation in o-xy plane fixed on the base of the module. The bending angle (θ) is the angle between the base and the top of the module. Constant curvature model assumes that the module bends with constant radius of r. According to [13] [24] the bending angle and orientation can be calculated as follows

$$\theta = \frac{2\sqrt{s_1^2 + s_2^2 + s_3^2 - s_1 s_2 - s_1 s_3 - s_2 s_3}}{3d} \tag{3.1}$$

$$\phi = tan^{-1}\left(\frac{\sqrt{3}(s_2 + s_3 - 2s_1)}{3(s_2 - s_3)}\right) \tag{3.2}$$

where d in the equation is the distance between the central axis of the module and the parallel strain gauges.

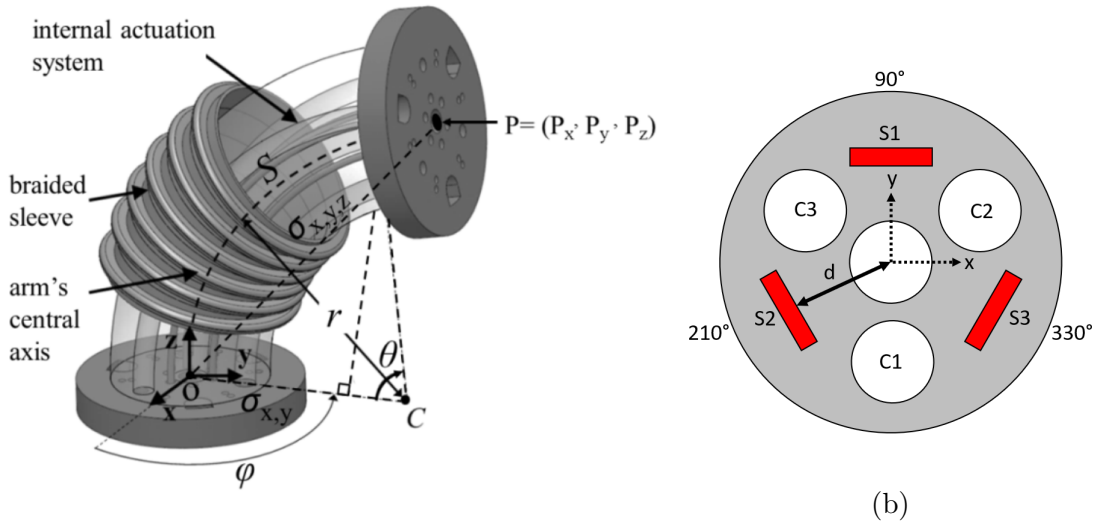

(a) (b)

Figure 3.6: (a) Three dimensional parameters of the module [23]. (b) Cross section view indicating the position of sensors and actuators.

3.4 RESISTANCE MODEL

The non-linear properties of ETPU makes it really hard to model how this material performs as a strain gauge. The model is separated into three parts, the basic strain gauge model, the resistivity change model, and the stress-strain relation of TPU model.

3.4.1 BASIC STRAIN GAUGE MODEL

The electrical resistance of a wire depends on its resistivity (ρ), length (L), and cross section area (A). The resistivity is the material property. The length and cross section area are geometric properties.

$$R = \frac{\rho L}{A} \tag{3.3}$$

The change of the resistance (ΔR) can be written as a partial derivative formula.

$$\Delta R = \frac{\delta R}{\delta L}\Delta L + \frac{\delta R}{\delta A}\Delta A + \frac{\delta R}{\delta \rho}\Delta \rho \tag{3.4}$$

$$= \frac{\rho}{A}\Delta L - \frac{\rho L}{A^2}\Delta A + \frac{L}{A}\Delta \rho \tag{3.5}$$

Using 3.3 and 3.5, the relative resistance change ($\frac{\Delta R}{R}$) can be written as follows

$$\frac{\Delta R}{R} = \frac{\Delta L}{L} - \frac{\Delta A}{A} + \frac{\Delta \rho}{\rho} \tag{3.6}$$

$$= (1 + 2v)\varepsilon + \frac{\Delta \rho}{\rho} \tag{3.7}$$

where v is Poisson's ratio and ε is the strain. The reasonable assumption of Poisson's ratio for TPU material is around 0.48 to 0.5 [22].

3.4.2 RESISTIVITY CHANGE MODEL

The sensor material in this research is thermoplastic polyurethane imbued with carbon black. Carbon black is a semiconductor that can improve the electrical conductivity of a base material [8]. As the implementation of the sensor in this experiment was not exposed to drastic temperature change, the resistivity change model in this chapter only assumes resistivity change caused by geometric change. A conductor has a band structure that describes the energy states that an electron is allowed or restricted to be in [6]. There are two bands that affected conductivity, valence band and conduction band. Conductor conductivity depends on its capacity to flow electrons from valence band to conduction band. The energy level gap between valence band and conduction band can be affected by strain. According to [2], the resistivity change is related to piezoresistive coefficient of the material (π) and contact stress (σ), the formula is as follows

$$\frac{\Delta \rho}{\rho} = \pi \sigma \tag{3.8}$$

$$= \pi E \varepsilon \tag{3.9}$$

where E is the Young's modulus.

Combining 3.7 and 3.9, the relative resistance change formula is as follows

$$\frac{\Delta R}{R} = (1 + 2v + \pi E)\varepsilon \tag{3.10}$$

3.4.3 STRESS-STRAIN RELATION OF TPU MODEL

The silicone module can be considered as a rod made from elastic material. According to Hooke's law, this can be viewed as a linear spring. The length change of the module (elongation) can be calculated as follows

$$\Delta L = \frac{F L_0}{A' E} \tag{3.11}$$

where F is the combined force from the pressure inside the three chambers, L_0 is the initial length, A' is the cross section area of the silicone part of the module (module cross section area minus area of three chambers), and E is the Young's modulus, and the final length can be calculated as $L = L_0 + \Delta L$. Assuming that the sensor elongates together with the silicone module, the length change of the module directly affects the length change of the sensor. According to constant curvature model [13], the length of the module is simply the average length of the three sensors.

$$L = \frac{s_1 + s_2 + s_3}{3} \tag{3.12}$$

Knowing the length of each sensor only by using the final length of the module is pretty hard. To simplify the modeling, the assumption is made that the closer the sensor to the activated chamber the more its length is affected by the length change of the silicone module. For example, using Figure 3.6, if c_1 is activated then the length of s_2 and s_3 increase with the same length change while s_1 retains its initial length.

3.5 ELECTRICAL MODEL

The simplest electrical circuit to measure resistance is a voltage divider circuit. The circuit produces output voltage that is a fraction of its input voltage. The fraction is a ratio between output resistance and total resistance. The circuit in this experiment is shown in Figure 3.7.

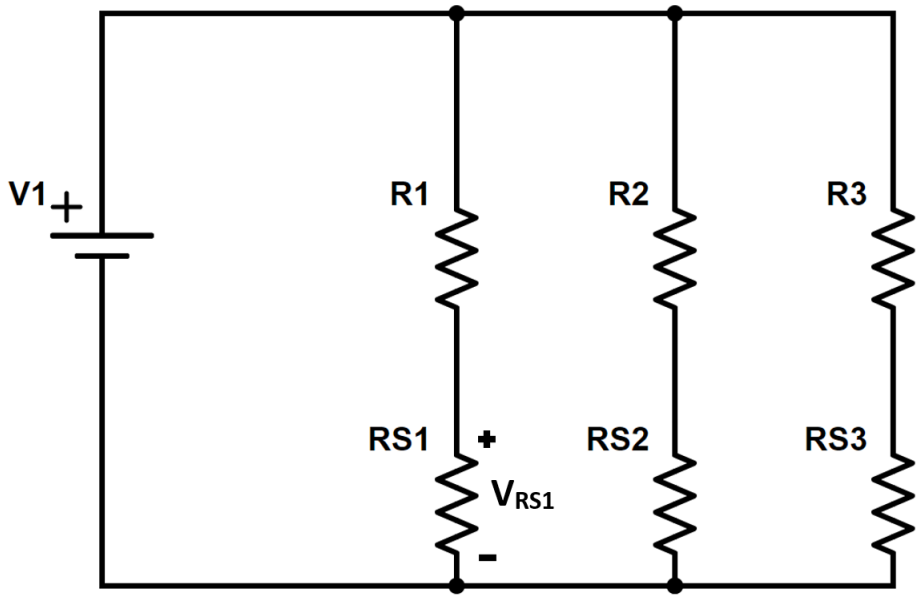

Figure 3.7: The schematic of voltage divider circuit used in this experiment.

The resistance of each sensor (RS_n) can be measured using formula below. The supply voltage (V_1) and three divider resistors (R_n) are known variables and determined by the user. The output voltage (V_{RS_N}) is measured.

$$V_{RSn} = \frac{RSn}{Rn + RSn} \times V_1 \tag{3.13}$$

$$RSn = \frac{Rn}{\frac{V_1}{V_{RSn}} - 1} \tag{3.14}$$

The implementation of the circuit to measure the resistance is shown in Chapter 5.

3.6 CONCLUSION

One of the important design factors for the sensor is the placement of the sensor relative to the module. There are three options, around the chambers, between the chambers, and outside the module. The second option was chosen. The first option needs better 3D printing method and equipment to achieve a spiral shaped sensor to wrap around the chambers. The third option needs a very thin sensor to be stuck to the module using adhesive. The alternative for the third option to place the sensor on the outer sheeting of the module is also not possible due to the wavy surface of the outer sheeting.

The shape of the 3D printed sensor is modified from the usual strain gauge shape. A wavy shape is implemented on the active grid section of the sensor to help the sensor "grips" the silicone. Constant curvature continuum robots modeling is used to model the kinematics of the module. This model utilizes the length of the sensors to determine the bending angle and orientation of the module. To model the change of the resistance, a combination of basic strain gauge model and resistivity change model is proposed. However, piezoresistive coefficient of the used material has not been researched thoroughly. The stress-strain relation of the sensor assumes that the sensors really elongate together with the module. Based on this assumption, the length change of the module directly affects the length change of the sensor. The length change of the module is modeled using Hooke's law for linear spring.

Chapter 4

FABRICATION

This part of the document explains the details of how the sensors and the endoscope module were made and assembled together.

4.1 MATERIALS

There were two main components used in this research, the silicone elastomer and the 3D printer filament. The tables below show the details of the available materials. The table is presented to show the compliance and durability of the available materials as those two characteristics are the basic requirements for sensing part in soft robotics.

Table 4.1: Available materials for the endoscope module.

NAME	SHORE HARDNESS	EQUIVALENCE[9]
Ecoflex™ 00-30	00-30	Gel shoe insole
Dragon Skin™ 10 FAST	10A	Rubber band

Table 4.2: Available materials for the sensors.

NAME	SHORE HARDNESS	ELONGATION AT BREAK	EQUIVALENCE[9]
X60	60A	700%	Tire tread
PI-ETPU 85-700+	85A	700%	Shoe heel
Eel NinjaTek	90A	355%	Shopping cart wheel
PI-ETPU 95-250	95A	250%	Shopping cart wheel
NinjaFlex SemiFlex	98A	200%	Shopping cart wheel

4.2 SENSOR

The sensor has two parts, the elastomer (red) and the conductive part (black). The conductive part was designed as a strain gauge and the elastomer was there to

keep the initial shape of the sensor while being assembled with the silicone module. The dimension of the sensor is shown in Figure 4.1. The length and width were chosen based on the maximum available space between the chambers and the printer resolution. The sensor should not be too thick that it will decrease the compliance of the module but also should be thick enough to not bend while being embedded into the module.

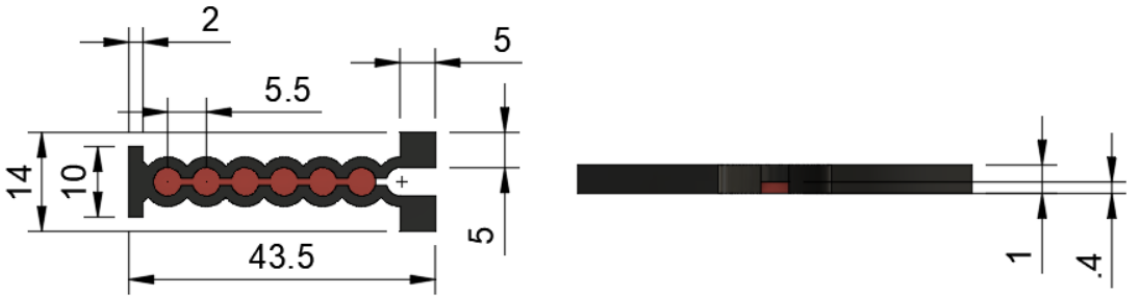

Figure 4.1: The dimension of the sensor in mm.

The chosen conductive filament for the sensor was PI-ETPU 85-700+. It has the lowest shore hardness and highest elongation at break; hence it was the most compliant and durable among available materials for this research. It also has good conductivity at $<500\,\Omega$cm. For the elastomer in this research, the best suited filament was NinjaFlex SemiFlex. Although X60 has lower shore hardness and better elongation at break, it did not stick really well with the PI-ETPU 85-700+.

The sensor was printed using Flashforge Creator Pro. The printer is equipped with flexion extruder to achieve better flexible material printing. The extruder is equipped with two nozzles which allows for two different materials printing. The diameter of the first nozzle is 0.4 mm and it was used to print the NinjaFlex SemiFlex filament. The diameter of the second nozzle is 0.6 mm and it was used to print the PI-ETPU 85-700+.

Simplify3D was used as the slicer for the 3D printing. The sensor was printed flat on the bed with a printing speed of 2000 mm/min. Both the NinjaFlex SemiFlex and the PI-ETPU 85-700+ were printed with the temperature of 220°C. The heating bed was kept at 60°C. The sensor was printed with 0.2 mm layer height. The conductive part was printed with two solid upper layers to give some space for the connection with the wire. The elastomer part was printed with only 20% infill so it did not add a lot of stiffness to the sensor as its purpose was only to maintain initial shape. The final result of the sensor is shown in Figure 4.2.

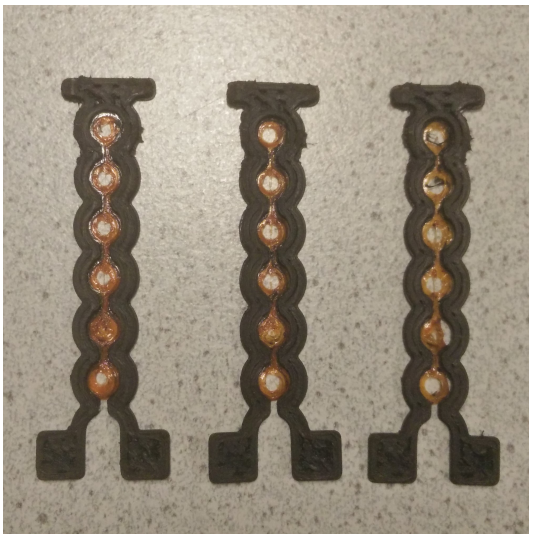

Figure 4.2: The 3D printed sensors.

4.3 ENDOSCOPE MODULE

The process of making the endoscope module consists of two parts, the body and the top. The body part was made using Ecoflex™ 00-30 and the top part is made using Dragon Skin™ 10 FAST. The mold parts for the silicone module is shown in Figure 4.3. The mold parts were 3D printed using VeroWhite and VeroClear materials [15]. Before the fabrication of the module, an easy-release agent was sprayed to the surface of the mold for easy release of the silicone from the mold.

The first step of the fabrication was to make the silicone mixture by combining Part A and Part B of the Ecoflex™ 00-30 with 1:1 weight ratio. After that the mixture was stirred thoroughly for 2-3 minutes and then vacuumed until all air bubbles were removed. The next step was to assemble mold part 1, 2, 4, 5, 6 and then place the sensors inside the mold. After the sensors were in place, the silicone mixture was poured into the mold. The silicone was cured after 4 hours. The steps are shown in Figure 4.4.

The next step of the fabrication process was to connect the sensors with the wires. This was done by soldering the wire into the bottom square part of the sensor. The soldering temperature was 300°C. By repeating the heating process using soldering iron, the wire went inside the bottom part of the sensor. This process should be done carefully because if not the structure of the sensor would be broken. The result after the soldering process is shown in Figure 4.5.

The top part was made using similar process as the body part. Dragon Skin™ 10 FAST mixture was used this time. It also has the same 1:1 weight ratio between Part A and Part B for the mixture. The mixture also went into the vacuum chamber to remove the air bubbles. The mold part 1, 3, 4, 5, 6 were assembled and the silicone module (body) was placed inside the mold. The silicone mixture was then poured into the mold (on top of the body part) and cured after 1.5 hours. The steps are shown in Figure 4.6.

After the top and body part of the module were done, the next step was to connect

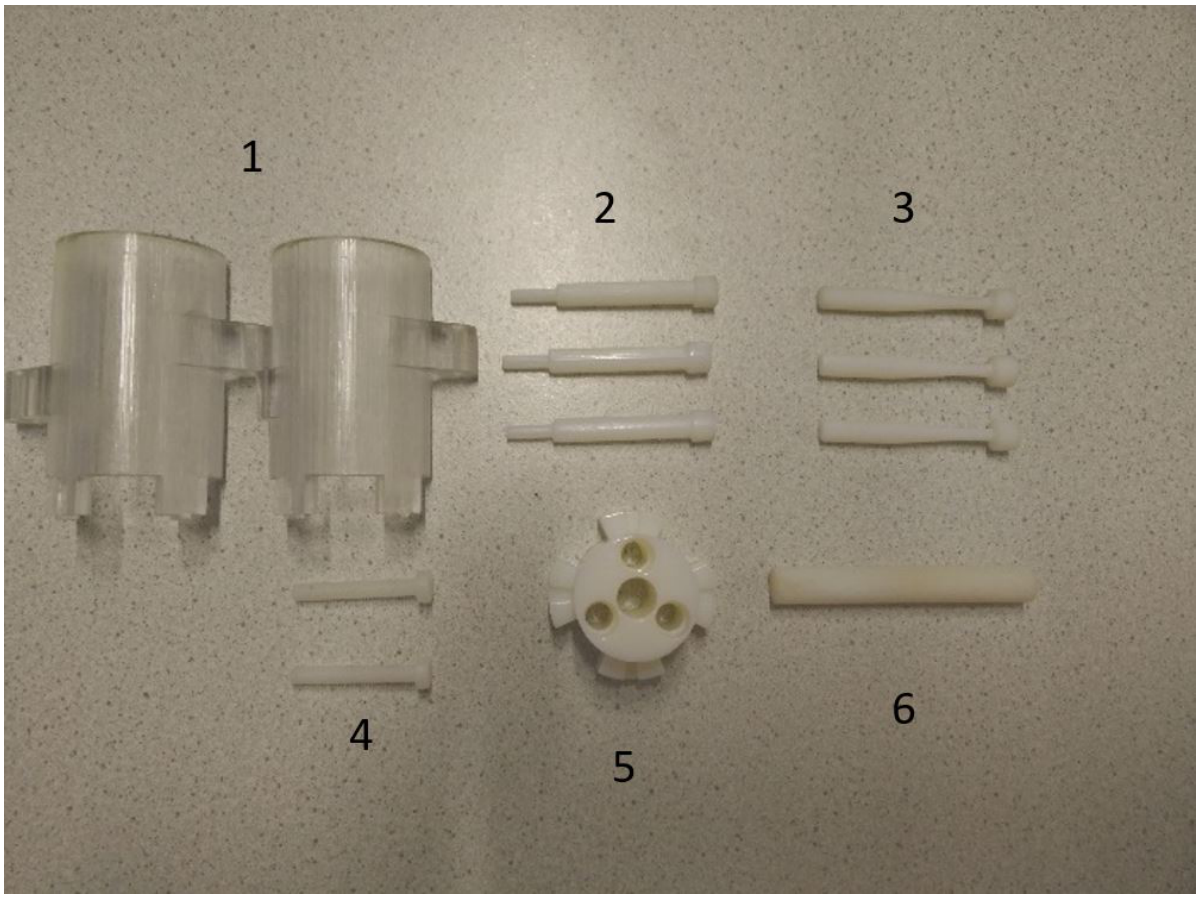

Figure 4.3: The mold parts for the endoscope module.

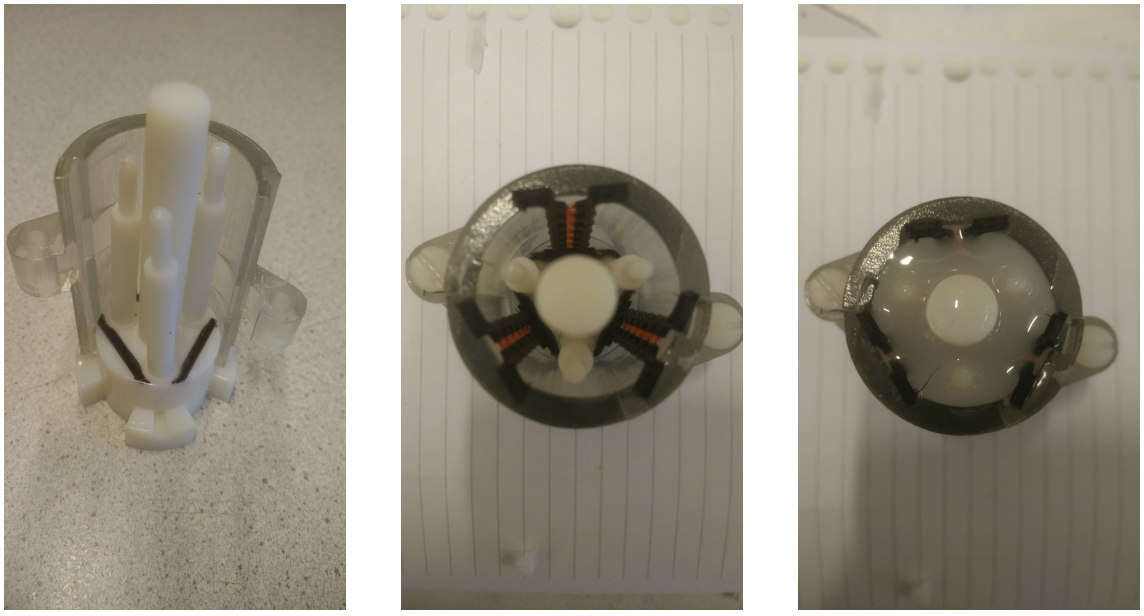

(a) (b) (c)

Figure 4.4: The fabrication steps of the body part with the sensors embedded into it.

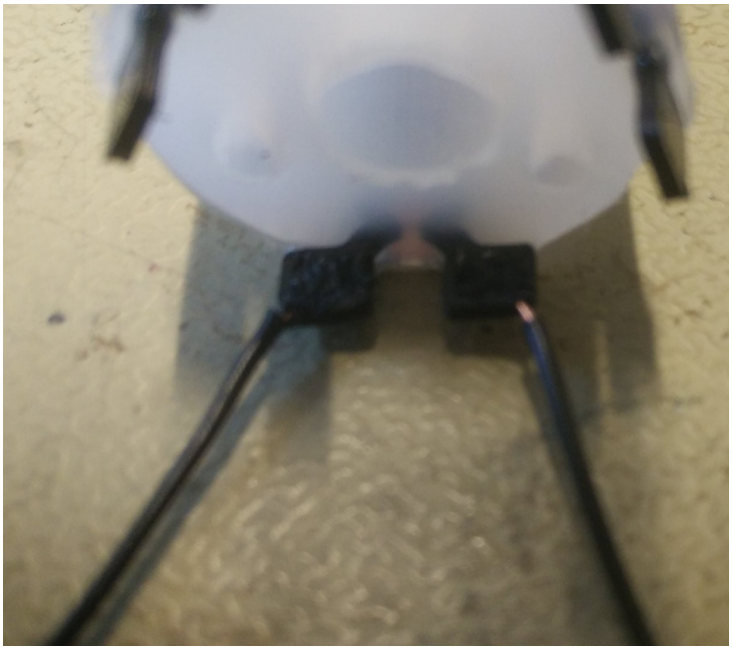

Figure 4.5: The wire connection of the sensor after soldering process.

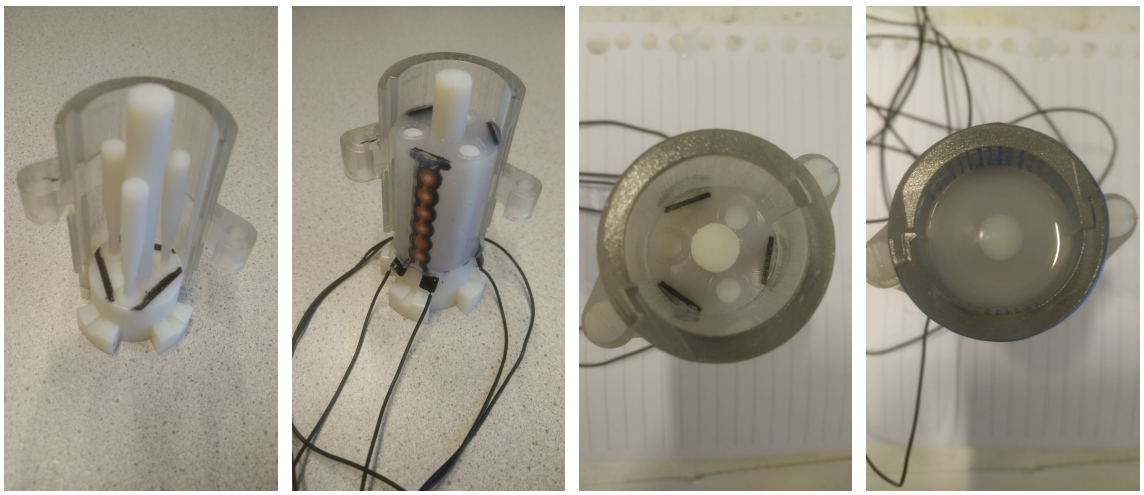

(a) (b) (c) (d)

Figure 4.6: The fabrication steps of the top part.

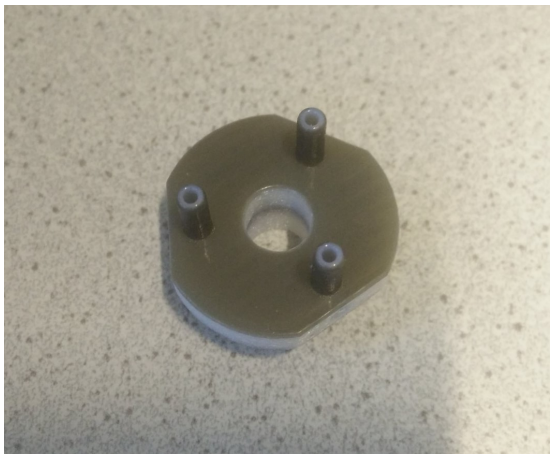

(a)

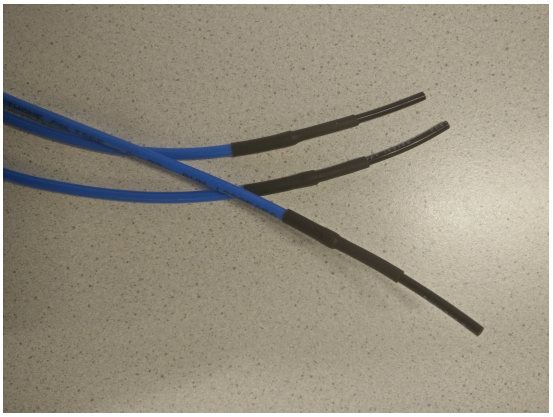

(b)

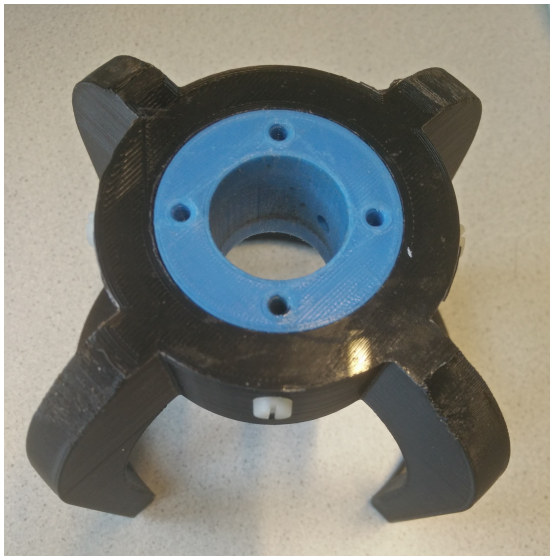

(c)

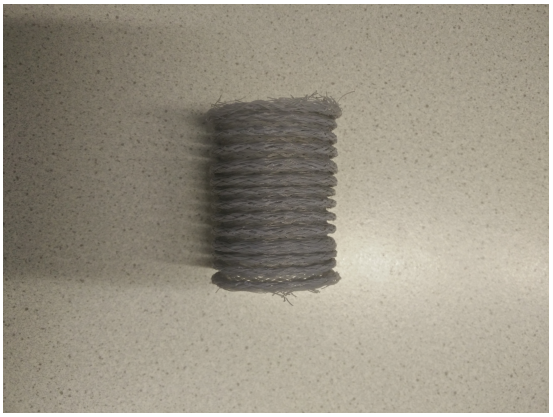

(d)

Figure 4.7: (a) Base part. (b) Pressure tubes. (c) Stand. (d) Braided sleeve.

the module with the pressure tubes. The base part of the module was 3D printed using PLA and connected to the pressure tube using super glue. The base part was then connected to the module bottom part also using super glue. The module was then placed at a stand printed using PLA to later make the measurement step easier. The printed base part also was placed at the top of the module to later serve as a holder for the EM tracker used for the validation experiments. Next, the module was wrapped with a braided sleeve to restrict the ballooning of the module. The braided sleeve was made by inserting a polyester sleeve around a metal rod with 40 cm diameter and then using a heat gun to give its structure [15]. The finished module is shown in Figure 4.8.

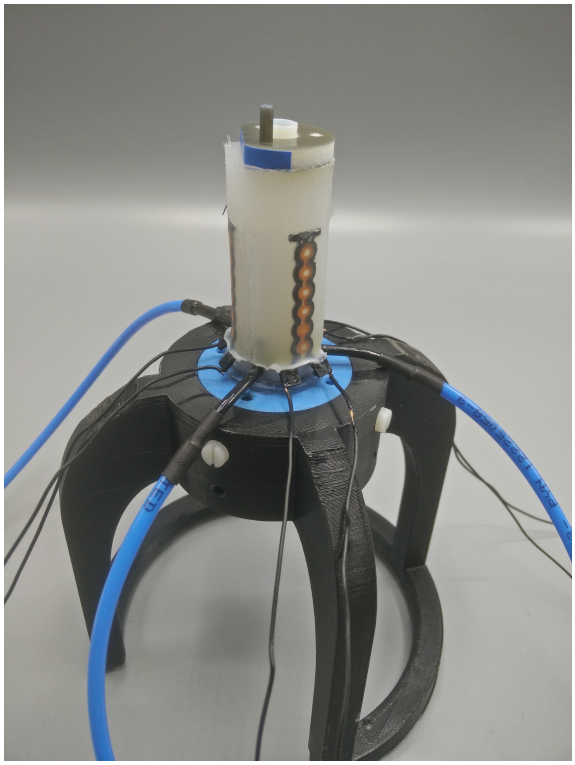

(a)

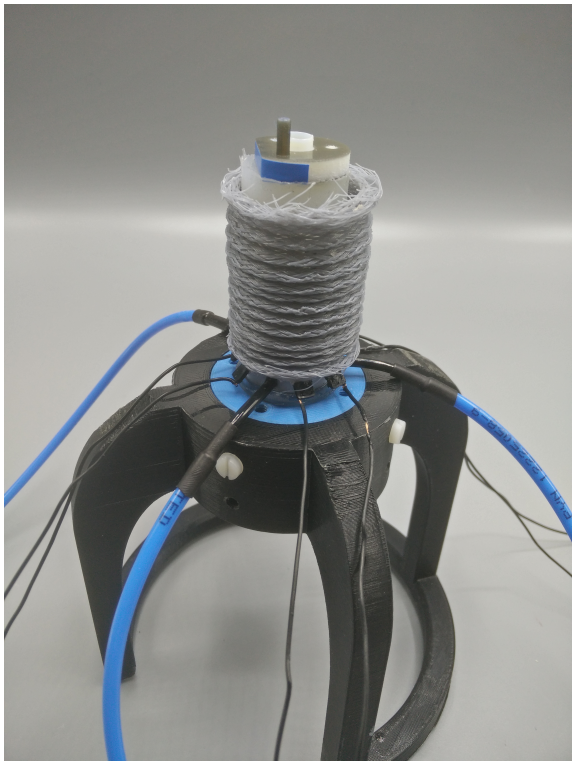

(b)

Figure 4.8: (a) Assembled module without the braided sleeve. (b) Assembled module with the braided sleeve.

4.4 CONCLUSION

The fabrication consists of two parts, the sensors and the module. The sensors fabrication was done by using FDM method with Flashforge Creator Pro printer. The most suitable 3D printing filament that is currently accessible for the conductive part is PI-ETPU85-700+ and NinjaFlex SemiFlex for the non-conductive part.

The module was made by molding silicone. Ecoflex™ 00-30 and Dragon Skin™ 10 FAST were used in this fabrication. The sensor was embedded into the module during the molding process; therefore, the sensors become the part of the module after the module was cured. The wire and pressure tube connection were assembled after that. The module was wrapped using polyester sleeve to constrict radial expansion and increase longitudinal expansion.

Chapter 5

EXPERIMENT SETUP

This chapter explains the purpose of the experiment and how the experiment was done.

5.1 AIM OF EXPERIMENT

There are two main purposes of the experiment. The first one is to characterize the elongation of the sensors inside the silicone module. The whole calculation of the bending revolves around the length of the sensor; therefore, it is important to know how the sensors elongate when the sensors are in contact with silicone. The second purpose of the experiment is to validate the usability of the length sensors to measure the bending of the module by comparing the processed data from the sensors with the ground truth (actual bending of the module).

5.2 SETUP

The general idea of the experiment was to actuate the endoscope module using pressure and then compare the processed data from the sensor with the electromagnetic (EM) tracker as the ground truth. The schematic is shown on Figure 5.1.

The soft endoscope module was actuated by pressuring the chambers inside. The pressure was limited and controlled using pressure regulator. The signal to control the pressure was sent via Arduino. The 3D printed sensors inside the silicone elongated as the module bent. The elongation resulted in resistance change of the sensors. By supplying the sensors with DC current, resistance change of the sensors translated into voltage change. The voltage was recorded using oscilloscope (PicoScope). The EM tracker also tracked and recorded the actual bending movement of the module. The data from the EM tracker were later compared to the processed data from the oscilloscope.

5.2.1 COMPONENTS

There are three main components for the experiment, the pressure regulator with Arduino shield, the EM tracker, and the oscilloscope.

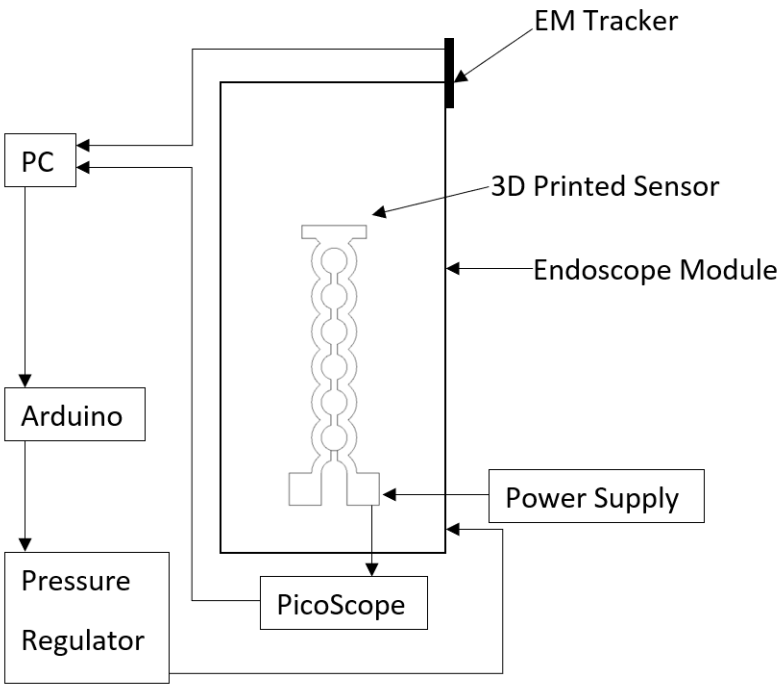

Figure 5.1: Schematic diagram of the experiment.

The pressure was regulated using Festo digital regulator (Figure 5.2a) which was connected with the Arduino shield (Figure 5.2b) to utilize PWM as the input signal from the user. Three pressure regulators were needed to actuate each chamber separately. Each regulator can give 1 bar output pressure at maximum and should not get more than 4 bar input pressure. The Arduino shield has the ability to control at maximum four pressure regulators at the same time and in this experiment three were used.

PicoScope 5443B (Figure 5.3a) was used to measure the voltage of the sensors. The sensors were supplied using external DC power supply. The resistance of each sensor was calculated using voltage divider circuit (Figure 5.3b). The voltage used in this circuit is 5V. The resistors used in this experiment had resistance around 10kΩ.

(a) (b)

Figure 5.2: (a) Three Festo pressure regulators. (b) Arduino pneumatic shield.

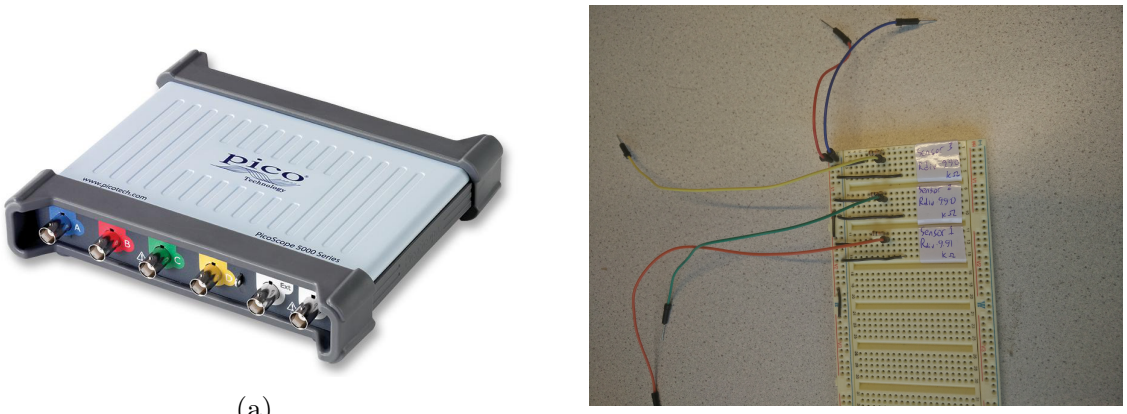

(a) (b)

Figure 5.3: (a) PicoScope 5443B. (b) Voltage divider circuit.

This value was picked to more or less match the resistance of the sensors; therefore, the measured voltage on the sensors were not to small or too big. The 3D printed sensors had resistance value around 8-15kΩ.

The EM tracker that was used in this experiment was NDI Aurora. This EM tracker consists of two parts, the tabletop field generator and the tracker. The tracker was placed on top of the endoscope module and then the endoscope module was placed on top of the field generator. The system control unit should be placed at least 1 meter from the field generator to prevent interference. The whole setup can be seen on Figure 5.4. The tracker at the top of the module is able to track its own position and rotation relative to the field generator. This function was then utilized to track the bending movement of the module. Using the rotation data of the tracker, the actual bending angle of the sensor was determined. The position of the tracker in the Cartesian coordinate system was used to determine the bending orientation of the module.

5.2.2 CONFIGURATION

There are seven types of actuation in the experiment.

1. Actuation of chamber 1, 2, and 3.
2. Actuation of chamber 1.
3. Actuation of chamber 2.
4. Actuation of chamber 3.
5. Actuation of chamber 1 and 2.
6. Actuation of chamber 2 and 3.
7. Actuation of chamber 1 and 3.

The first actuation resulted in the vertical elongation only of the module. This configuration enabled the elongation characterization of the sensors because each sensor only elongated in vertical direction. The rest of the actuation resulted in the

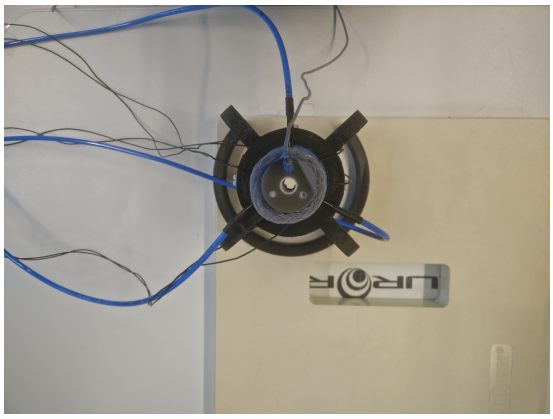

(a)

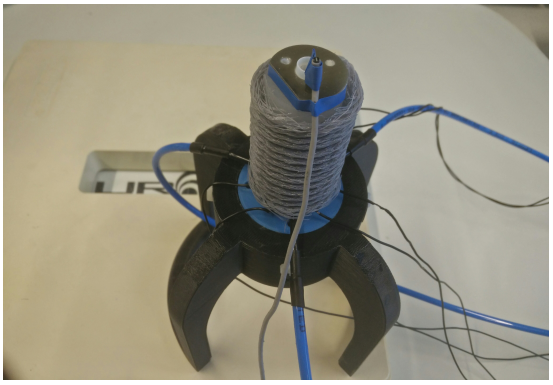

(b)

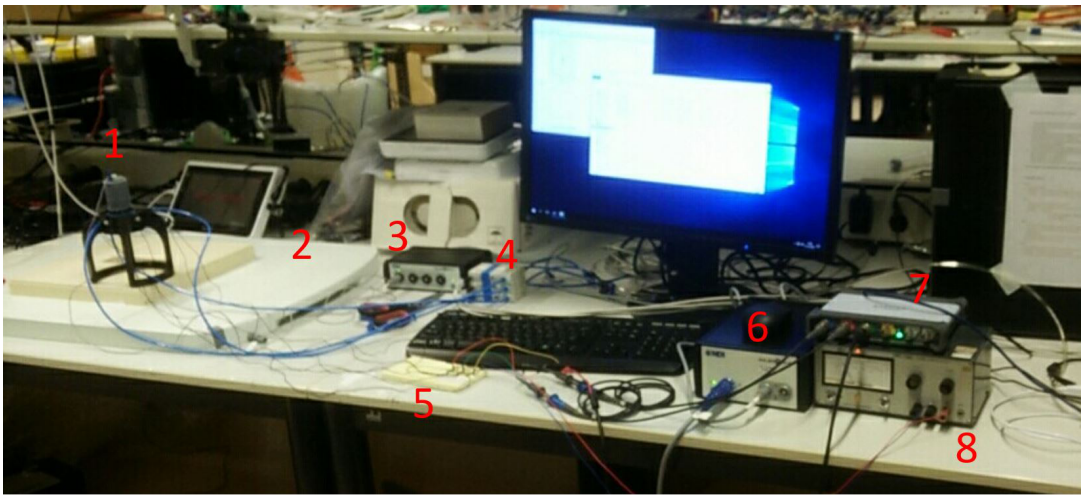

(c)

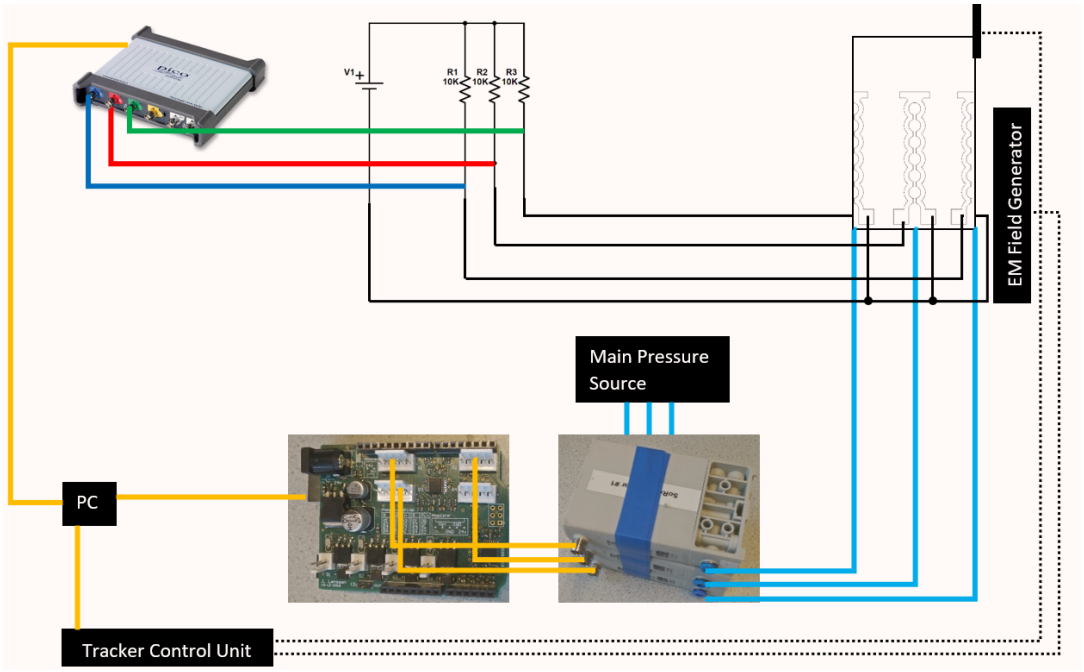

(d)

Figure 5.4: (a) Top view of the system. (b) Side view of the system. (c) The whole view of the setup [(1) Module with EM tracker (2) Field generator (3) Interface unit (4) Pressure regulators with Arduino shield (5) Voltage divider (6) System control unit (7) PicoScope (8) DC power supply]. (d) The whole setup as a schematic connection drawing.

bending of the module. The direction (orientation) of the bending depends on which chamber(s) is(are) actuated. The maximum pressure that can be handled by the module is 0.3 bar. The pressure was increased from 0 to 0.3 bar with $\frac{1}{255}$ or ≈0.004 bar step every 100 ms and then decreased from 0.3 to 0 bar with the same step at the same time interval. The initial plan according to the requirement was to use 0.4 bar however the module was damaged at that pressure (Appendix B). The EM tracker was recording the translation and the rotation of the top part of the module with sampling frequency of 40 Hz. The voltage change from the sensor recorded using PicoScope with sampling frequency of 100 Hz. Each type of actuation was performed for 120 seconds. The data from the PicoScope and the data from the NDI Aurora were synchronized, filtered, and processed later using MATLAB.

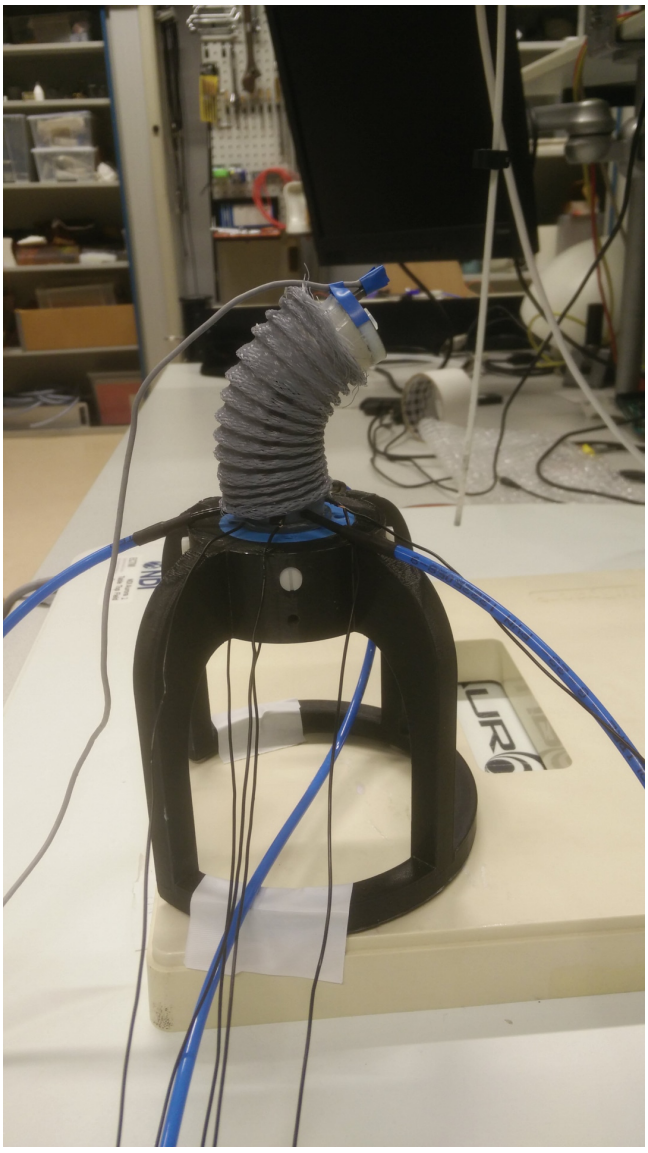

Figure 5.5: Bending movement of the module.

5.3 DATA PROCESSING

This section explains how the obtained data were processed to produce the results in the next chapter.

5.3.1 SYNCHRONIZATION

There were two data sets gathered from two different measurement devices, PicoScope and EM tracker. These data sets had different sampling rate and timestamp. Synchronization between the data sets was needed before comparing them. The synchronization was done by resampling the data sets on the time range where the two data sets overlap. The resampling used the higher sampling frequency between the two and linear interpolation to fill the data sets.

5.3.2 FILTERING

The data set from the PicoScope had noise and drift. To get better insight from the data, filtering was needed. Drifting is usually caused by a lower frequency component and noise is originated from higher frequency component. To filter both noise and drift, a band-pass filter was made. The cutoff frequencies were designed by first looking at the dominant frequencies of the data using Fourier analysis and then choosing the frequency range with desired amplitude.

5.4 CONCLUSION

The experiment was done to characterize the sensor elongation inside the silicone module and then to validate the usability of the length sensors to measure the bending movement of the module. By pressuring all three chambers at the same time, the module elongates on the vertical direction. Pure elongation from this activation is used to characterize each sensor.

The bending measurement was done by pressuring one or two chambers at the same time to achieve a bending movement. The pressure to activate the module was controlled using three pressure regulators, one for each chamber. The data from the length sensors were compared to the data from the EM tracker as the ground truth. The length sensors data were first synchronized with the data from the EM tracker and then filtered using band-pass filter to remove undesired characteristics (noise and drift).

Chapter 6

RESULTS AND DISCUSSIONS

The sensor characterization and validation were both done three times. This section presents only the second trial because it has the best results. The other results can be seen on Appendix C.2. The first part of this chapter contains the characterization of each sensor and the sensor usability validation on the second and third part.

6.1 DRIFT AND NOISE REMOVAL

The obtained data from the PicoScope contains drift and noise. To remove the drift and noise, band-pass filter was implemented. To choose the cutoff frequencies (lower cutoff frequency and upper cutoff frequency), the raw data was analyzed using Fourier analysis. This process helps to determine the dominant frequencies on the data. It can be seen from Figure 6.1 that there are several frequencies with relatively high magnitude especially between 0.009 Hz and 0.252 Hz.

The lowest frequency that is still relevant is 0.063 Hz which is close to the chamber activation frequency (0.065 Hz). The highest frequency that still has relatively big magnitude is around 0.2 Hz. The chosen lower cutoff frequency for the band-pass filter is 0.06 Hz and 0.2 Hz for the upper cutoff frequency. The filtered data (Figure 6.2) is relatively smoother and not drifting as much compared to the raw data.

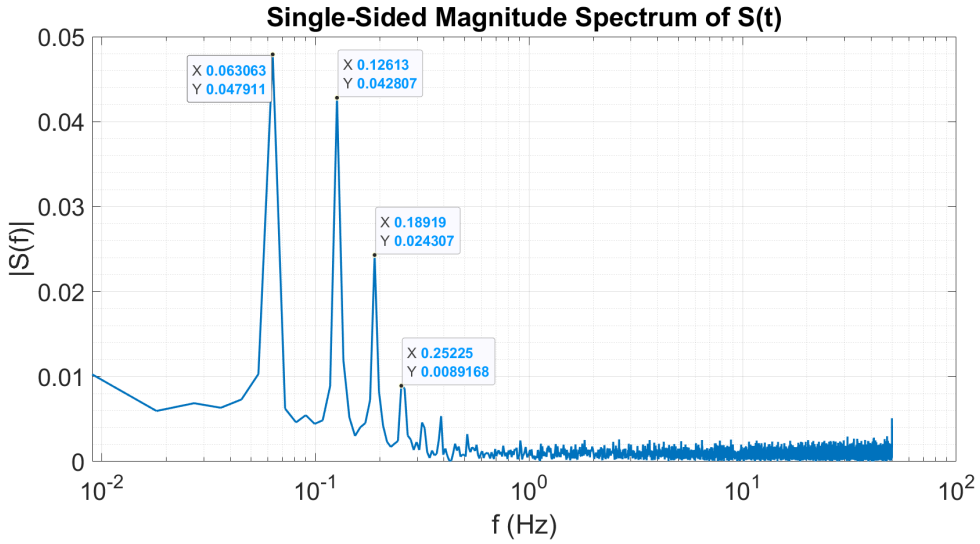

Figure 6.1: Single-sided magnitude spectrum from the raw data.

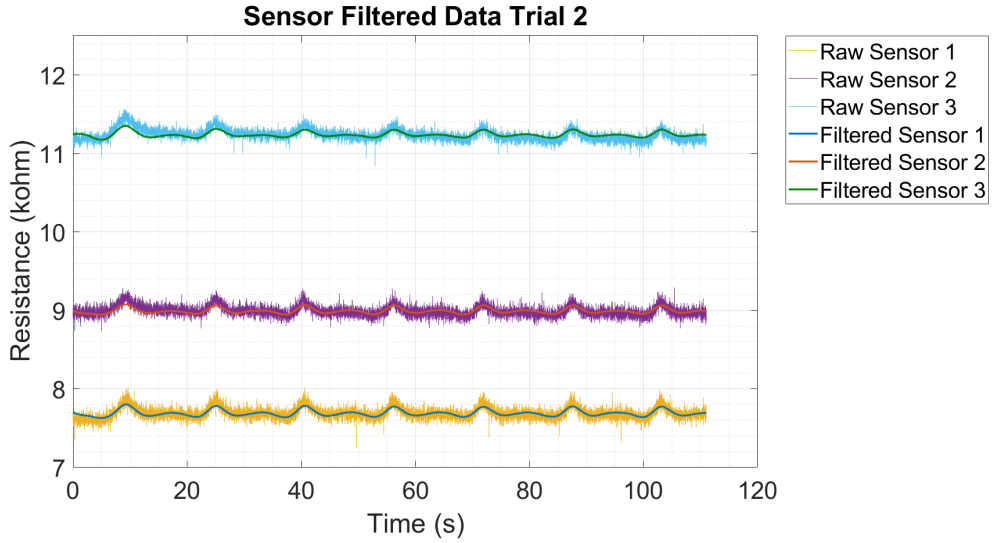

Figure 6.2: The filtered data using band-pass filter.

6.2 SENSOR CHARACTERIZATION

The data was obtained by elongating the module vertically; therefore, the next step to characterize the sensors is by comparing the filtered data with the elongation of module. It can be seen from Figure 6.3 that the synchronization between the data from the sensor and from the EM tracker worked well. This comparison however cannot give enough insight on how the elongation affect the resistance. To be get better comparison, relative resistance change, instead of resistance value, is compared to the elongation (Figure 6.4).

Figure 6.4 shows that the resistance drops at the start of the elongation. The resistance then increases and decreases following the elongation. Near the end of the elongation cycle, the resistance increases again before it drops again at the beginning of the next elongation cycle. The elongation data also has some drifting

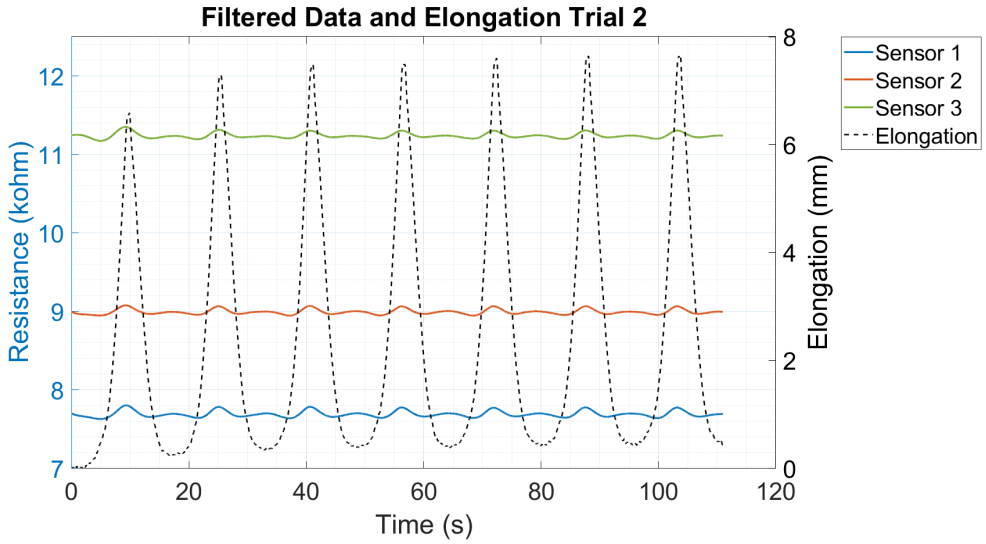

Figure 6.3: Resistance value compared to the elongation of the module.

that might be caused by the module itself or the placement of EM sensor on top of the module.

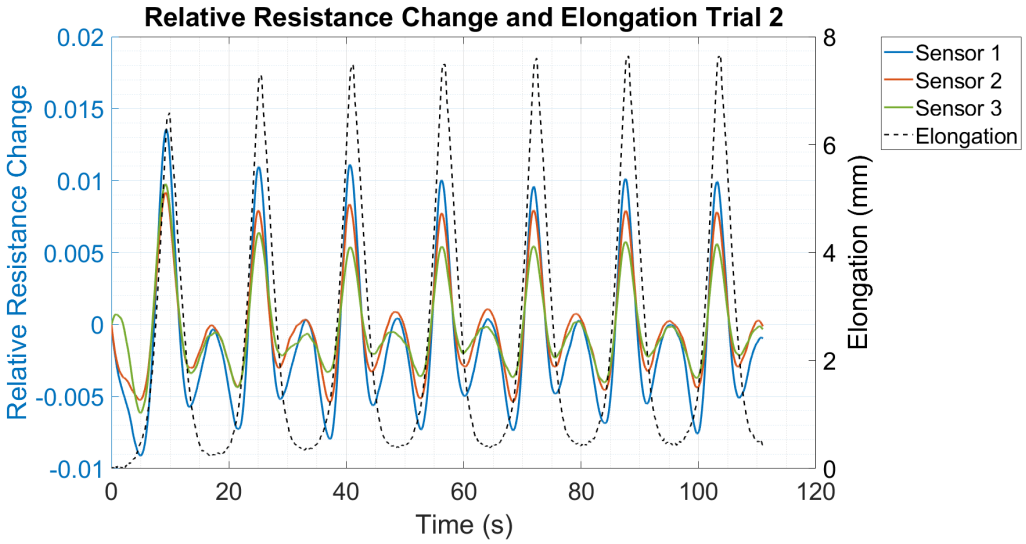

Figure 6.4: Relative resistance change compared to the elongation of the module.

To help find the relation between the elongation and the relative resistance change, as explained on Equation 3.10, Figure 6.4 is made into hysteresis curve. This hysteresis curve is then curve-fitted using MATLAB. It is clear that the hysteresis curve is not linear as modeled in Equation 3.10. To be able to capture the increase and decrease phase of the hysteresis curve, second order polynomial is used for curve-fitting. The curve-fitting process ignores the first cycle of the elongation because, as can be seen from the hysteresis curve, it was activated more than the other cycles. It gives some insight on the characteristic of the ETPU material that it needs time to reach a steady state. The fitted curve is constrained to go through the lowest relative resistance change for each sensor. The second order fitting however is not really optimal to capture the characteristic of the sensor.

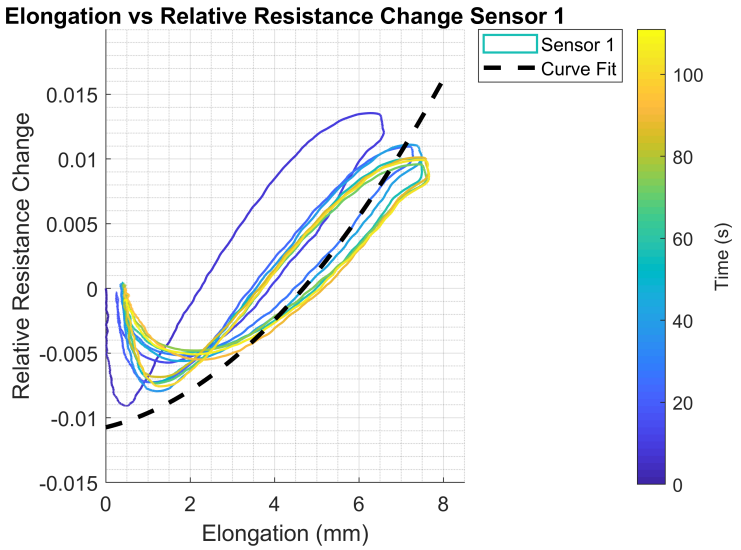

(a)

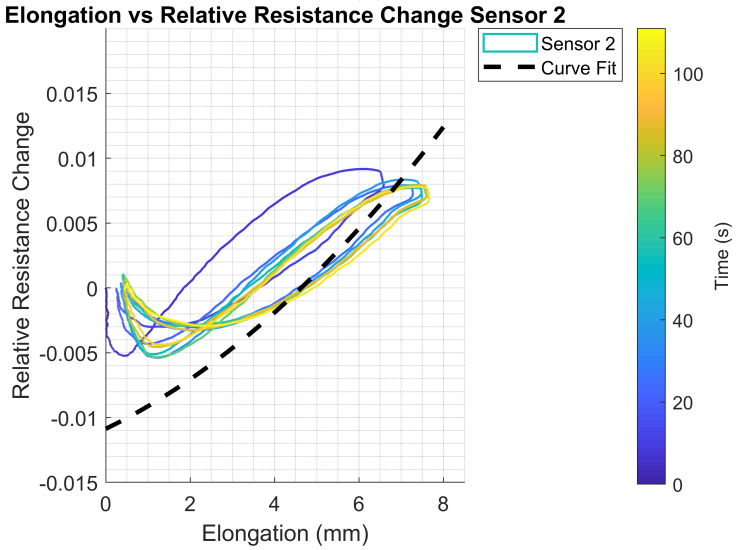

(b)

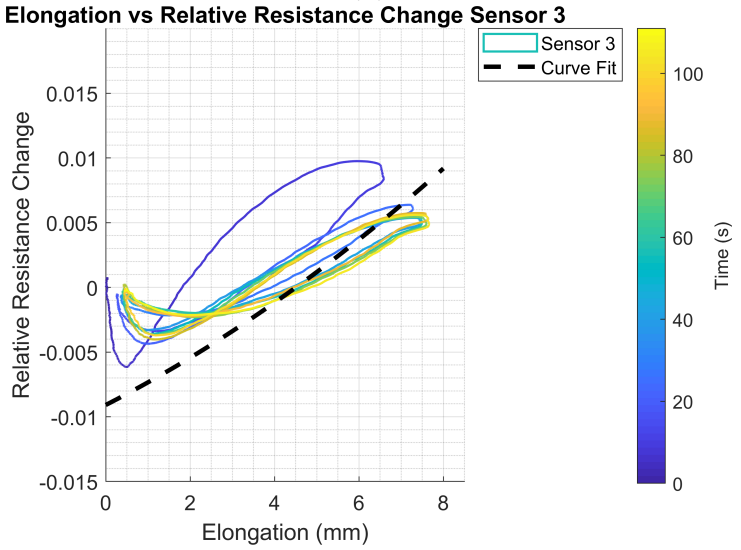

(c)

Figure 6.5: Hysteresis curve with curve-fitted graph.

6.3 BENDING ANGLE VALIDATION

The obtained equation is used to calculate elongation using relative resistance change of each sensor from experiment configuration 2 to 7. This elongation is converted into bending angle using Equation 3.1.

The vertical elongation resulted from activating chamber 1,2, and 3 at the same time should only produce a very little bending angle. As can be seen from Figure 6.6g, that the true bending angle obtained from EM tracker is only around 1°. The bending angle calculated from the sensors also shows small bending angle (below 5°) with overshoot at the beginning of the elongation cycle.

The achievable bending angle using the STIFF-FLOP module is 70° to 80° for single chamber activation at 0.3 bar [15]. However, the combination between the module and the sensors in this research reduces the achievable bending angle to be around 9° to 25° (69% to 87% reduction).

Figure 6.6a, 6.6b, and 6.6c show that the maximum errors between bending angle measured using the 3D printed sensors and the EM tracker range from 7.11°to 23.32°. The two chambers activation setup, as can be seen from 6.6d, 6.6e, and 6.6f, shows maximum errors ranged from 1.62°to 10.26°.

The result from the first trial and third trial also show the same pattern (Appendix C.2 and D.2). The maximum errors for each configuration and trial are shown below excluding the first bending cycle. The maximum error keeps getting bigger after each usage of the module. The maximum error is often not at the peak of the curve (maximum bending angle) but at the slope and the maximum error is almost always more than 100%.

Table 6.1: Maximum errors between 3D printed sensors and EM tracker.

	Trial 1	Trial 2	Trial 3
Chamber 1	7.60°	9.54°	11.09°
Chamber 2	4.76°	7.11°	6.35°
Chamber 3	19.65°	23.32°	22.72°
Chamber 1 and 2	4.99°	1.62°	2.48°
Chamber 1 and 3	12.31°	10.26°	12.16°
Chamber 2 and 3	4.02°	4.11°	4.42°

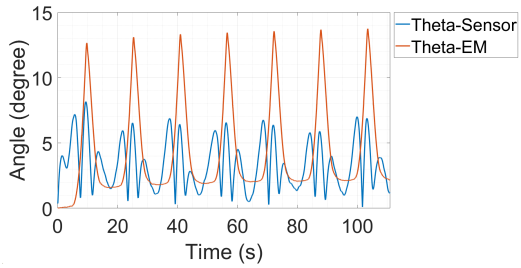

(a) Chamber 1

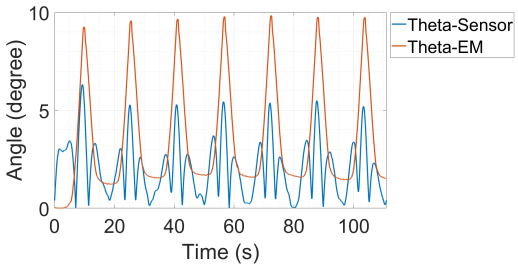

(b) Chamber 2

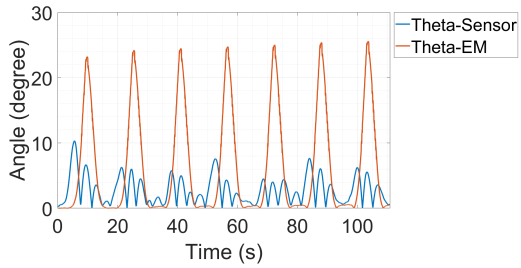

(c) Chamber 3

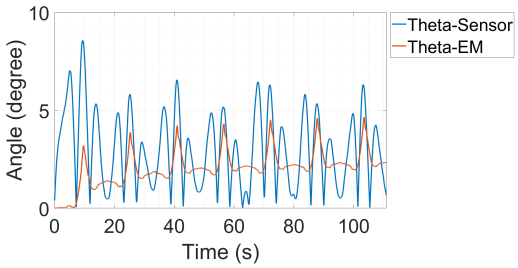

(d) Chamber 1 and 2

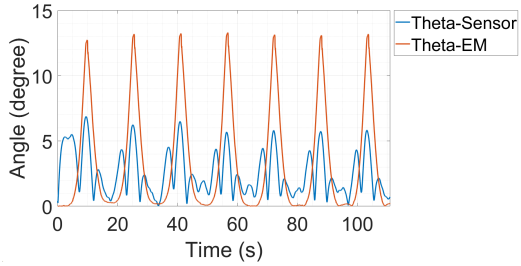

(e) Chamber 1 and 3

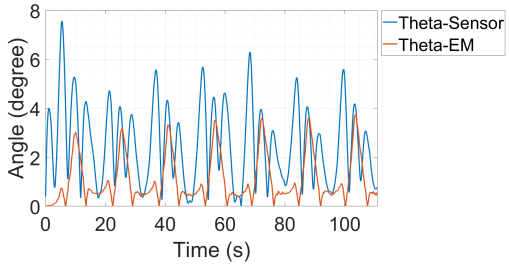

(f) Chamber 2 and 3

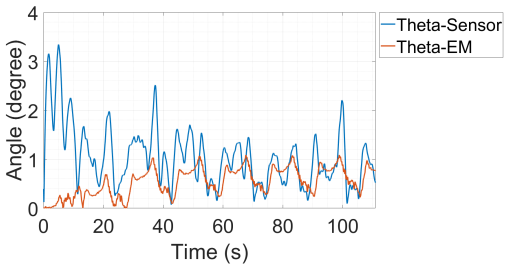

(g) Chamber 1, 2, and 3

Figure 6.6: Validation of bending angle from the 3D printed sensors with bending angle from the EM tracker.

6.4 ORIENTATION VALIDATION

The orientation angle is calculated using Equation 3.2. The orientation of the module is where the module is facing, seen from the top, while being actuated. Using Figure 3.6 as a reference, the expected orientation angles for each activation are as follows:

- 90° if chamber 1 is activated.
- 210° if chamber 2 is activated.
- 330° if chamber 3 is activated.
- 150° if chamber 1 and 2 are activated.
- 30° if chamber 1 and 3 are activated.
- 270° if chamber 2 and 3 are activated.

It can be seen from the results measured using EM tracker that the orientation of the module is pretty close to the expectation except for when chamber 1 and 3 and chamber 2 and 3 were activated together. This is also the case for the first and third trial. This suggests that the activation of each chamber is not equal especially chamber 3. The orientation angle calculated from the 3D printed sensor does not really show any clear orientation of the module.

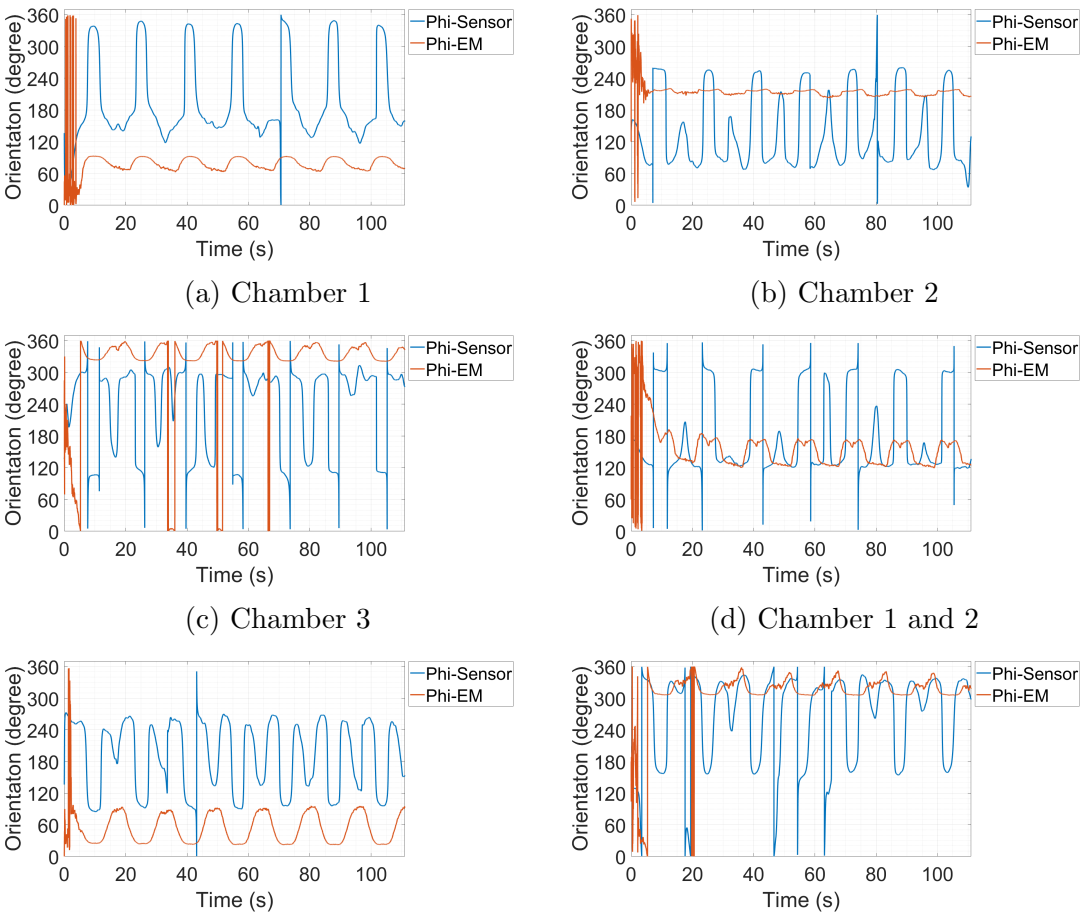

(a) Chamber 1

(b) Chamber 2

(c) Chamber 3

(d) Chamber 1 and 2

(e) Chamber 1 and 3

(f) Chamber 2 and 3

Figure 6.7: Validation of orientation angle from the 3D printed sensors with orientation angle from the EM tracker.

However, by using the relative resistance change of each sensor, the orientation angle of the module can be guessed roughly. As stated in Chapter 3.4.3, each activated chamber results in different activated sensors. For example, if chamber 1 is activated, then sensor 2 and 3 are activated more than sensor 1. The behaviors of the sensors for each configuration are shown below.

Table 6.2: Expected sensor activation behaviors for each chamber activation.

	Sensor 1	Sensor 2	Sensor 3
Chamber 1	Less	More	More
Chamber 2	More	Less	More
Chamber 3	More	More	Less
Chamber 1 and 2	Less	Less	More
Chamber 1 and 3	Less	More	Less
Chamber 2 and 3	More	Less	Less

For the activation of chamber 1, chamber 2, chamber 3, chamber 1 and 2, and chamber 2 and 3, the data match the expected behavior. However, for the activation of chamber 1 and 3, the relative resistance change of sensor 1 is supposed to be closer to sensor 3 rather than sensor 2. Although, the data still match the expected behavior that sensor 2 is activated more than sensor 1 and sensor 3. From the relative resistance change data, the activated chamber is known and the direction where the module is facing can be guessed.

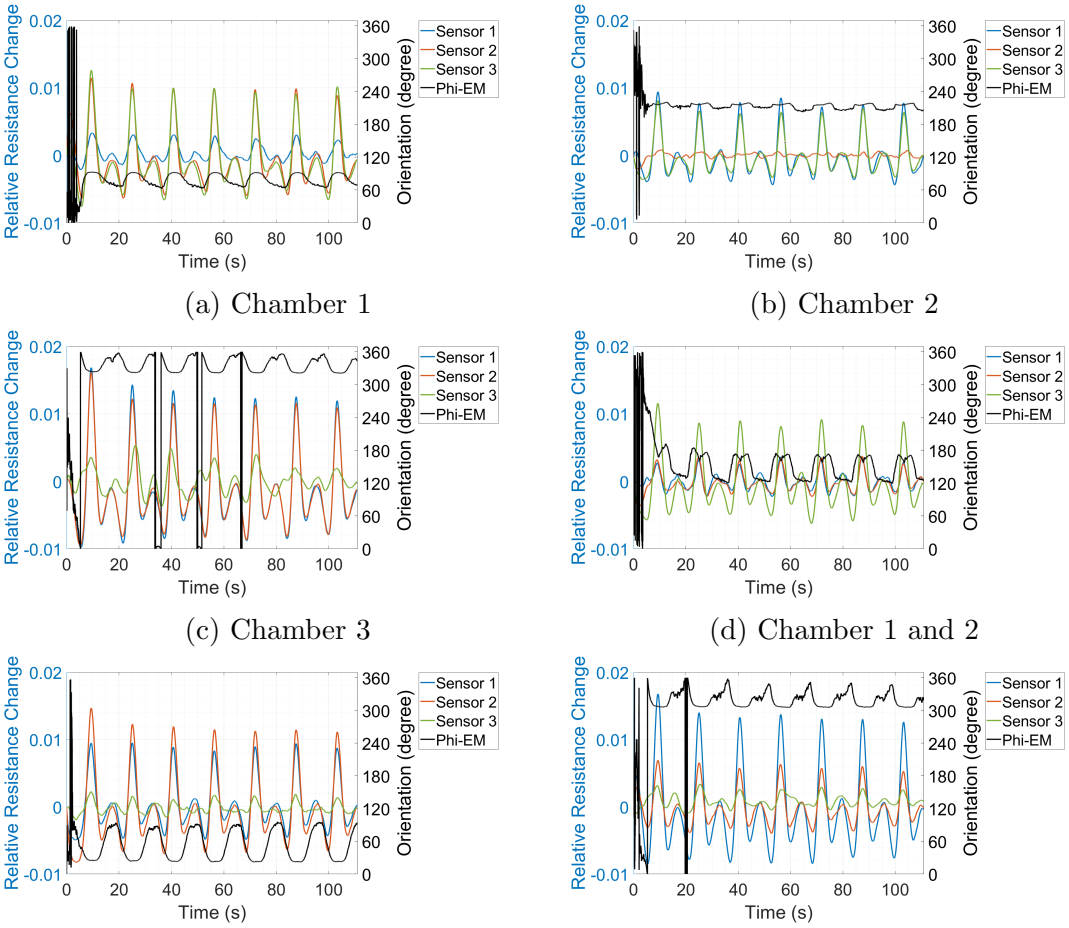

(a) Chamber 1

(b) Chamber 2

(c) Chamber 3

(d) Chamber 1 and 2

(e) Chamber 1 and 3

(f) Chamber 2 and 3

Figure 6.8: Relative resistance change data for each chamber activation compared with orientation angle from the EM tracker.

6.5 DISCUSSIONS

Figure 6.4 shows that the resistance is always dropping at the start of elongation cycle. It results in a small peak between each elongation cycle. According to [5], there are two main processes happening simultaneously when conductive composite is subjected to strain, breakdown and formation of conductive networks.

The resistance dropping might be the effect of more dominant breakdown than formation. Near the end of each elongation cycle, the resistance starts increasing again to a certain value. This suggests that when the composite reverts back to its original shape, the formation of conductive networks is more dominant than the breakdown. This breakdown and formation of the conductive networks affect the change of the resistivity of the composite. This breakdown and formation of conductive networks are affected by the strain rate. At higher strain rate, the breakdown processes are more dominant for the most part. The breakdown and formation balance each other at lower strain rate resulting in only small effect in increasing resistivity of the composites. Low strain rate in this case is as low as 0.1 mm/min and the strain rate in this research is around 62.4 mm/min. This suggests that the resistivity change model in Equation 3.10 cannot be ignored.

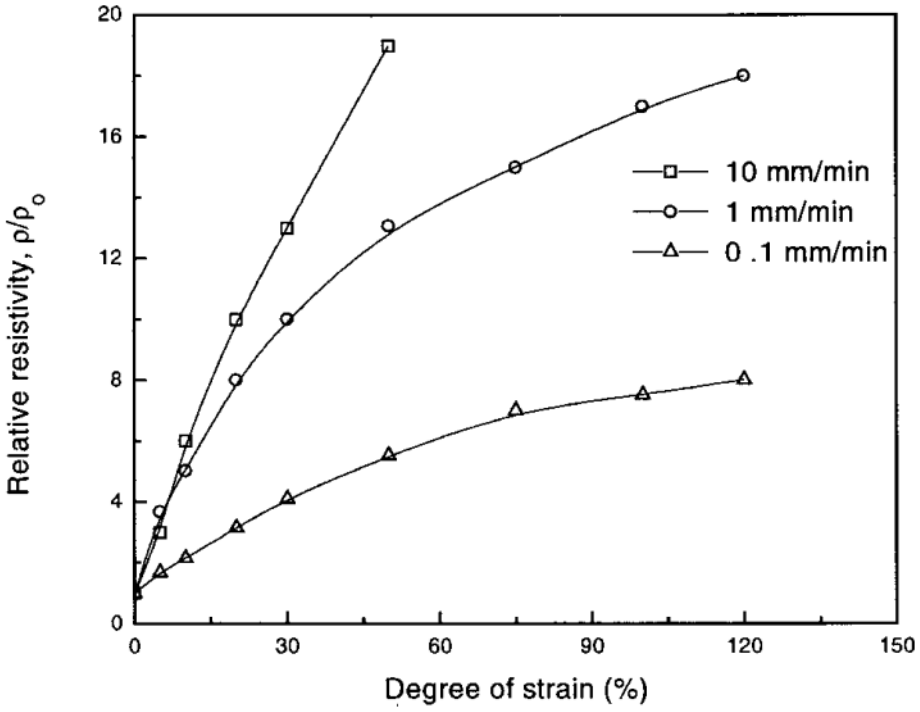

Figure 6.9: The resistivity of the composite is affected by its strain rate [5].

Embedding the sensor inside the module apparently might also be a problem. Based on how the chamber(s) is(are) inflating when actuated, the center of the module is shifting and changing the distance between the sensors and the center of the module [14]. This distance, as stated in Equation 3.1, is needed to calculate the bending angle. The inflation between the chambers is also not uniform, this might affect how the sensors are strained inside the module. The strain sensed by the sensors

is not only the desired elongation but also the inflation of the chambers. The characterization of the sensors using only elongation of the module, as can be seen in Figure 6.4, is not the best approach.

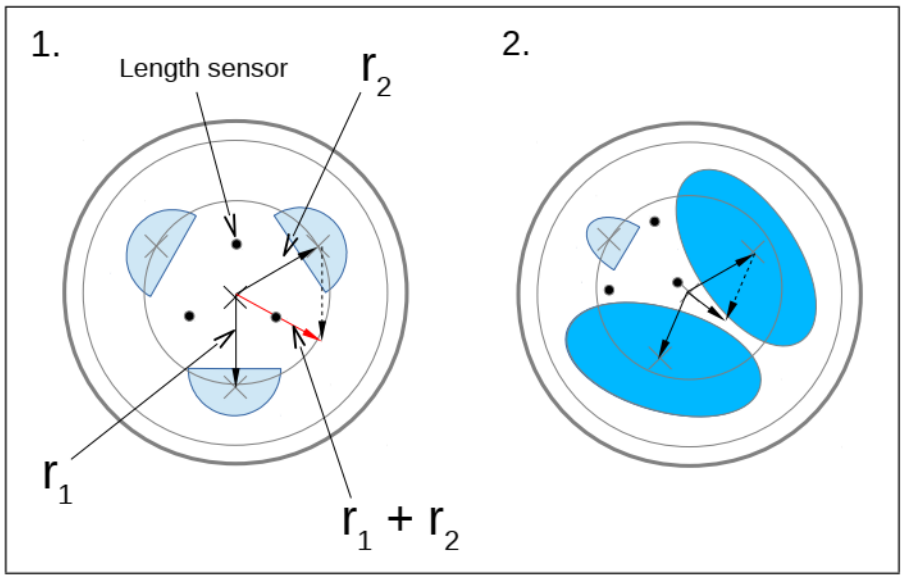

Figure 6.10: The internal inflation of the chambers shifts the center of the module [14].

Chapter 7

CONCLUSIONS AND RECOMMENDATIONS

7.1 CONCLUSIONS

The purpose of this research is to find a way to utilize FDM 3D printing methods to develop sensors to measure bending and orientation angle of endoscope module. Three fully 3D printed resistive length sensors made of conductive and non-conductive TPU were successfully manufactured and embedded inside the endoscope module. The sensors position utilizes empty space between the chambers and does not interfere with the hollow center part of the module reserved for other medical or optical devices.

The development of the sensors was only implemented and validated on one module and not multi modules. The sensors were not tested in different environment conditions; therefore, it is not known if the performance of the sensors is affected by conditions such as temperature and vibration.

The sensors add more stiffness to the endoscope module and reduce the achievable bending by 69% to 87%. The sensors also limit the module maximum pressure to only 0.3 bar from previously 0.4 bar. Each sensor has each own measurement; therefore, there are two wires installed for each sensor which means 6 wires per endoscope module.

The strain-dependent resistance characteristic of the sensors were not successfully modeled using basic strain gauge model and stress-strain relation of the TPU. The stress-strain relation of the TPU assumes that the strain is only elongation which is probably not given how the chamber is also inflating while elongating. The basic strain gauge model only takes dimensional change and not material change, it does not take into account the resistivity change caused by strain. The piezoresistive coefficient of the used conductive TPU needs further study knowing that the resistivity of the material is also affected by strain rate. As a result, the model is unable to characterize the conductive TPU material.

The bending angle measured by the 3D printed sensors has significant error, it is more than 100% for the most part. With the assumption that all of the chambers are equal, the error value between each chamber activation should be close. However, the achieved angle and the error value differs. This suggests that the manual

manufacturing process of the sensors and the module (e.g. placing the sensors inside the mold, pouring the silicone) might contribute to the error. The orientation angle calculation does not really tell the orientation of the module. Instead, the resistance data from the 3D printed sensor shows which chamber(s) is(are) activated and gives rough idea where the module is currently facing.

7.2 RECOMMENDATIONS

There are three things that can be improved on the next project. The first improvement recommendation is for the type of the sensor. The approach of using resistive sensor for more straight forward measurement did not really pan out well to address the non-linearity. Changing the approach by using capacitive sensor might be helping the linearity and repeatability of the sensor [25].

Different placement of the sensor should also be considered. Placing the printed sensors on top of the braided sleeve (outside the module) might help limiting the strain that affects the sensors to only elongation because the inflating is already constricted by the sleeve. It also helps to retain the distance (d) between the central axis of the module and the sensors.

The last thing that could be revised is the measurement method. It is known that the ETPU has rate dependant hysteresis and needs time to reach steady state. Discrete measurement might be better in the next development to at least know if the sensor can measure the angle. For example, actuating the module to reach 5°, calculating the measured angle by the sensors, then continue actuating to 10°, and so on.

Bibliography

[1] A. Abbas and J. Zhao. "Twisted and Coiled Sensor for Shape Estimation of Soft Robots". In: *International Conference on Intelligent Robots and Systems* (2017).

[2] A. Alvin Barlian et al. "Review: Semiconductor Piezoresistance for Microsystems". In: *IEEE* (2009).

[3] M. Bartlett, E. Markvicka, and C. Majidi. "Rapid Fabrication of Soft, Multilayered Electronics for Wearable Biomonitoring". In: *ADVANCED FUNCTIONAL MATERIALS* (2016).

[4] H.G.D. Braakman. "Magnetic Field Sensing on 3D Printed Structures". MA thesis. the Netherlands: University of Twente, 2019.

[5] N.C. Das, T.K. Chaki, and D. Khastgir. "Effect of Axial Stretching on Electrical Resistivity of Short Carbon Fibre and Carbon Black Filled Conductive Rubber Composites". In: *Polymer International* (2002).

[6] S. Dhar. "Analytical Mobility Modeling for Strained Silicon-Based Devices". PhD thesis. Vienna: Technischen Universität Wien, 2007.

[7] A. Dijkshoorn et al. "Embedded sensing: integrating sensors in 3-D printed structures". In: *JSSS* (2018).

[8] Jean-Baptiste Donnet. *Carbon Black. Science and Technology*. Marcel Dekker, Inc., 1993.

[9] *Durometer Shore Hardness Scale*. URL: https://www.smooth-on.com/page/durometer-shore-hardness-scale/.

[10] K. Elgeneidy et al. "Directly Printable Flexible strain sensors for Bending and contact Feedback of soft actuators". In: *Frontiers in Robotics and AI* (2018).

[11] M. Gifari et al. "A Review on Recent Advances in Soft Surgical Robots for Endoscopic Applications". In: *The International Journal of Medical Robotics and Computer Assisted Surgery* (2018).

[12] C. Huber et al. "3D print of polymer bonded rare-earth magnets, and 3D magnetic field scanning with an end-user 3D printer". In: *Applied Physics Letters* (2016).

[13] R.J. Webster III and B.A. Jones. "Design and Kinematic Modeling of Constant Curvature Continuum Robots: A Review". In: *The International Journal of Robotics Research* (2010).

[14] F. Jan and M. Cianhetti. "New STIFF-FLOP Module Construction Idea for Improved Actuation and Sensing". In: *IEEE International Conference on Robotics and Automation* (2015).

[15] J.W. Lageveen. "Developing a Path Planning Algorithm to Enhance the Performance of a Soft Robotic Endoscope". MA thesis. the Netherlands: University of Twente, 2019.

[16] M. Luo et al. "Toward Modular Soft Robotics: Proprioceptive Curvature Sensing and Sliding-Mode Control of Soft Bidirectional Bending Modules". In: *SoRo* (2017).

[17] H. Naghibi et al. "Development of a Multi-level Stiffness Soft Robotics Module with Force Haptic Feedback for Endoscopic Applications". In: *International Conference on Robotics and Automation* (2018).

[18] S. Ozel et al. "A Composite Soft Bending Actuation Module with Integrated Curvature Sensing". In: *International Conference on Robotics and Automation* (2016).

[19] T. Pereira, S. Rusinkiewicz, and W. Csail. "Computational Light Routing: 3D Printed Optical Fibers for Sensing and Display". In: *ACM Transactions on Graphics* (2014).

[20] T. Pinto et al. "CNT-based sensor arrays for local strain measurements in soft pneumatic actuators". In: *International Journal of Intelligent Robotics and Applications* (2017).

[21] P. Polygerinos et al. "Soft Robotics: Review of Fluid-Driven Intrinsically Soft Devices; Manufacturing, Sensing, Control, and Applications in Human-Robot Interaction". In: *ADVANCED ENGINEERING MATERIALS* (2017).

[22] H.J. Qi and M.C. Boyce. "Stress-Strain Behavior of Thermoplastic Polyurethane". In: *Mechanics of Materials* (2004).

[23] S. Sareh et al. "Macrobend optical sensing for pose measurement in soft robot arms". In: *Smart Materials and Structures* (2015).

[24] S. Sareh et al. "Pose Sensor for STIFF-FLOP Manipulator". In: *IOP Publishing* (2018).

[25] J. Shintake et al. "Ultrastretchable Strain Sensors Using Carbon Black-Filled Elastomer Composites and Comparison of Capacitive Versus Resistive Sensors". In: *ADVANCED MATERIALS TECHNOLOGIES* (2018).

[26] *Strain Gauges*. URL: https://www.continuummechanics.org/straingauges.html.

[27] S. Wakimoto, J. Misumi, and K. Suzumori. "New concept and fundamental experiments of a smart pneumatic artificial muscle with a conductive fiber". In: *Elsevier* (2016).

[28] H. Wang, M. Totaro, and L. Beccai. "Toward Perceptive Soft Robots: Progress and Challenges". In: *Advanced Science* (2018).

[29] *What is TPU and ETPU?* URL: https://rubber3dprinting.com/what-is-tpu/.

[30] K. Willis et al. "Printed Optics: 3D Printing of Embedded Optical Elements for Interactive Devices". In: *UIST* (2012).

[31] Y. Xu et al. "The Boom in 3D-Printed Sensor Technology". In: *MDPI* (2017).

[32] H. Zhao et al. “Optoelectronically innervated soft prosthetic hand via stretchable optical waveguides”. In: *Science Robotics* (2016).

Appendix A

FIRST DESIGN TRIAL

The most achievable shape using the printer was a tube with spiral direction printing. To be able to print a spiral shape, a solvable support material is needed. It is not really clear in Figure A.2 but the tube shaped sensor was not really embedded into the silicone module. The sensor easily came off with only a little force.

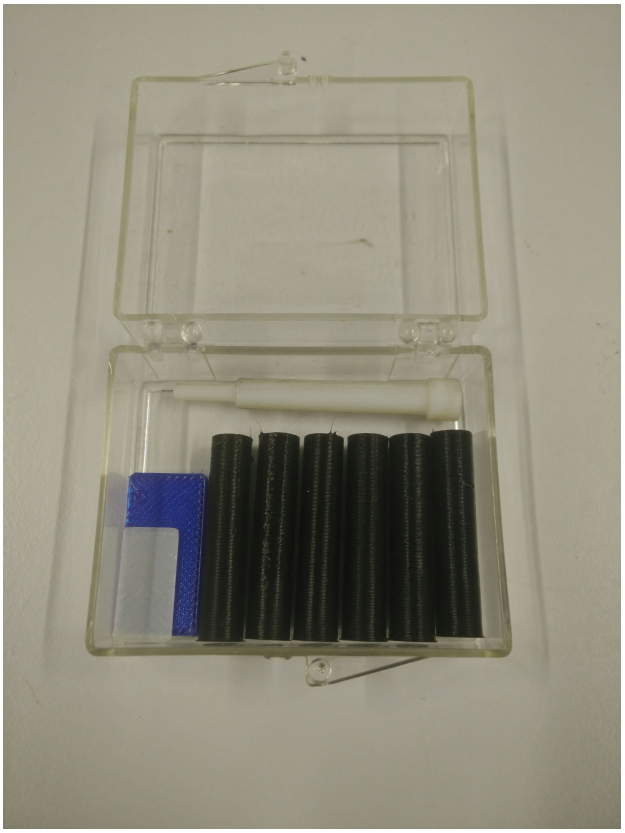

Figure A.1: The first sensor fabrication trying to achieve spiral shape.

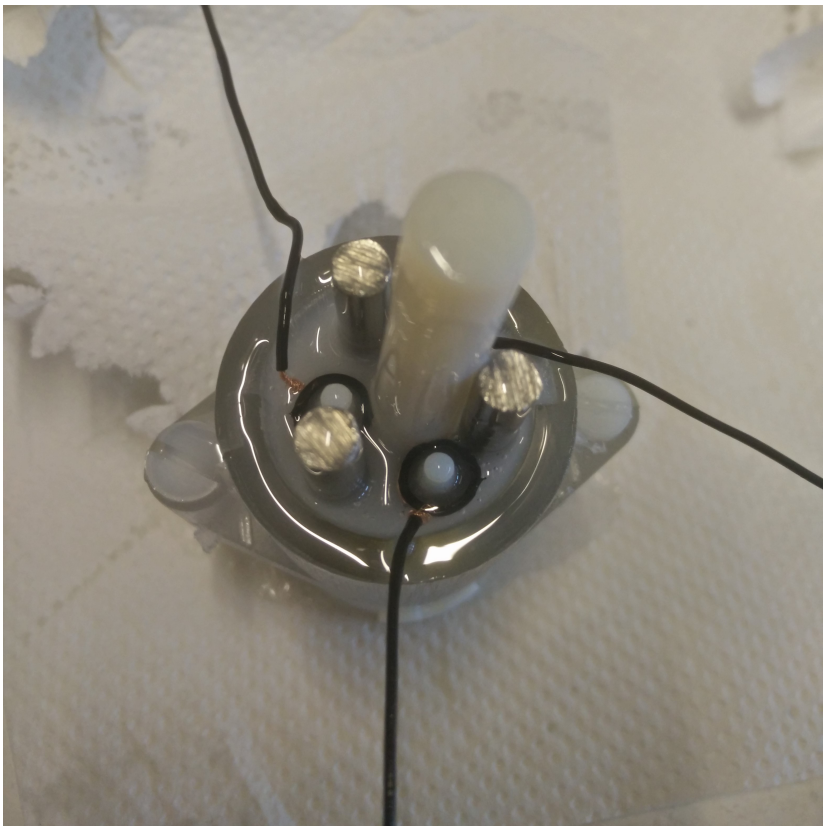

Figure A.2: The first module fabrication with embedded sensor.

Appendix B

DAMAGED MODULE

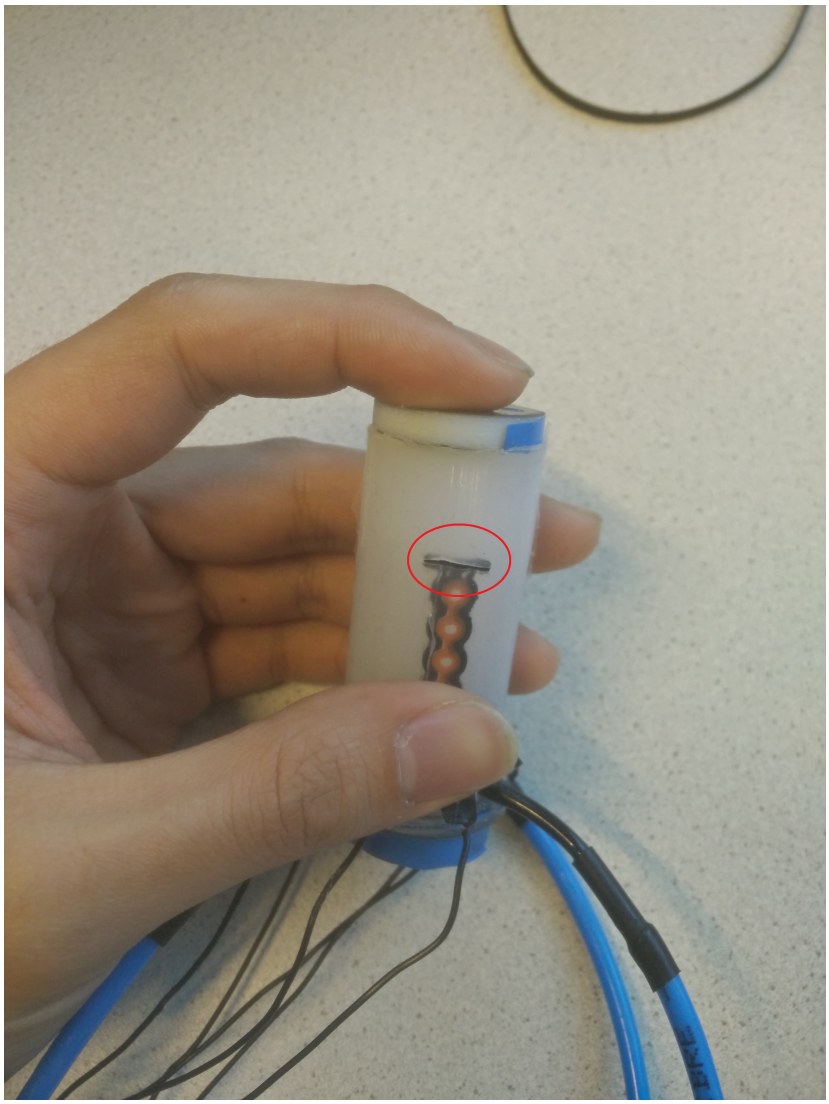

Figure B.1: Small cut resulting in pressure leakage on the silicone module when 0.4 bar was applied.

Appendix C

THE FIRST TRIAL RESULTS

C.1 Bending Angle

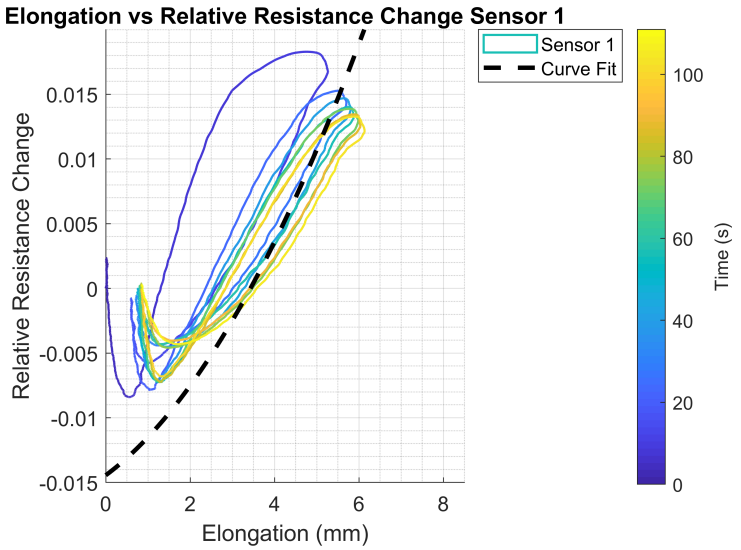

(a)

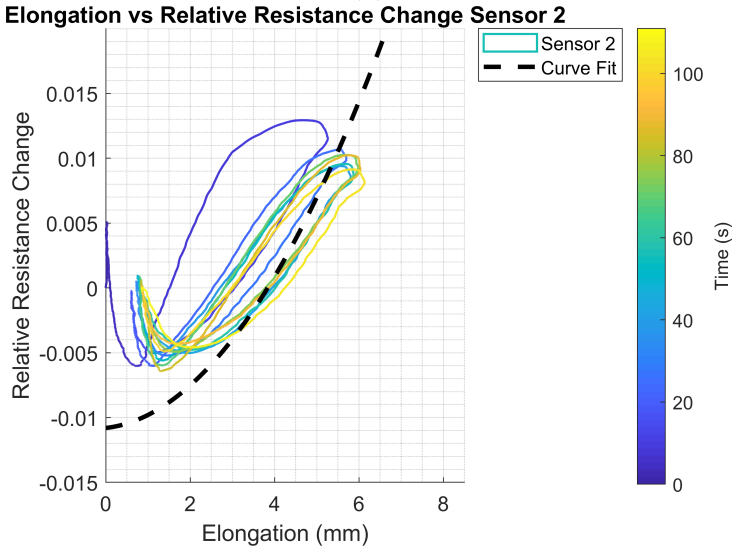

(b)

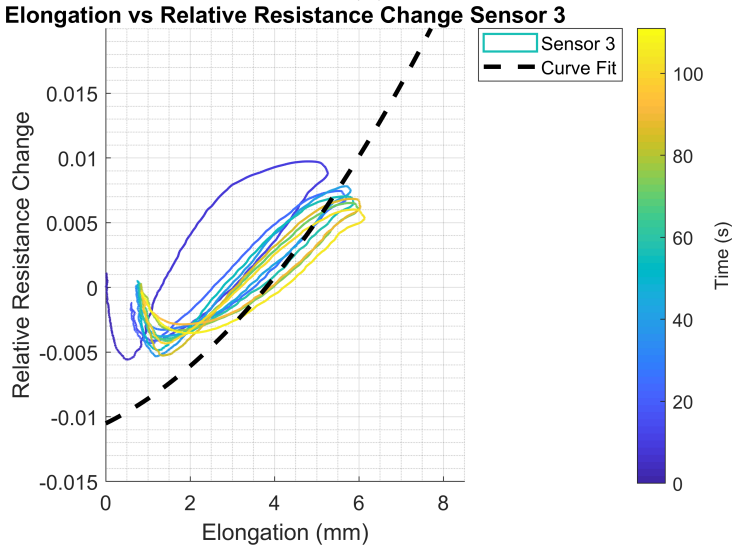

(c)

Figure C.1: Hysteresis curve with curve-fitted graph from trial 1.

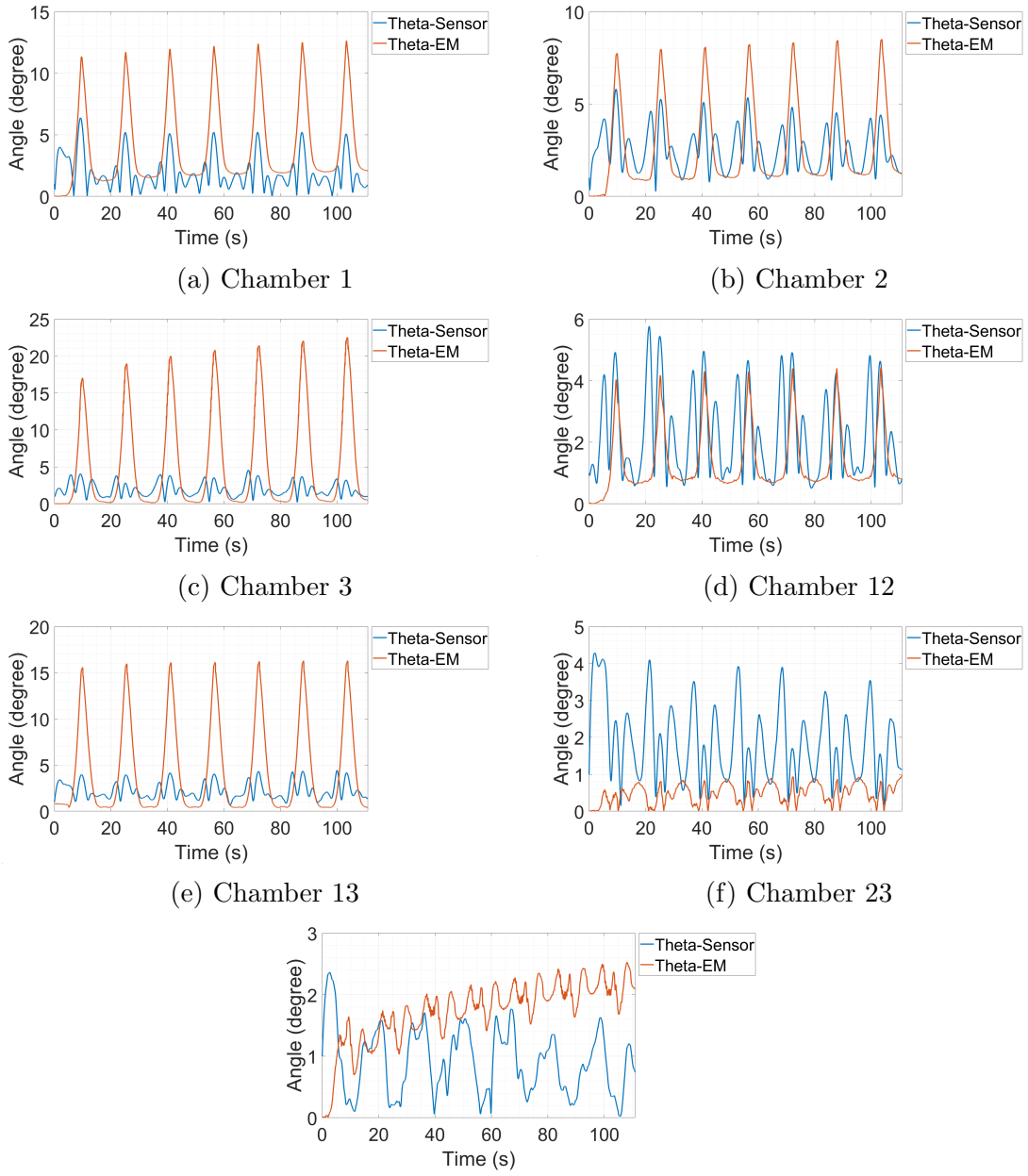

(a) Chamber 1

(b) Chamber 2

(c) Chamber 3

(d) Chamber 12

(e) Chamber 13

(f) Chamber 23

(g) Chamber 123

Figure C.2: Validation of bending angle from the 3D printed sensors with bending angle from the EM tracker (trial 1).

C.2 Orientation Angle

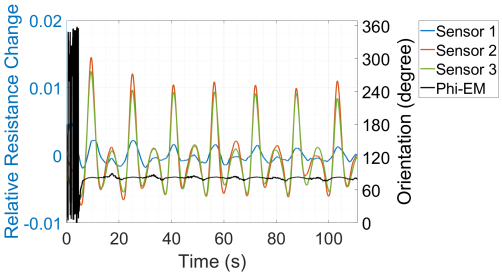

(a) Chamber 1

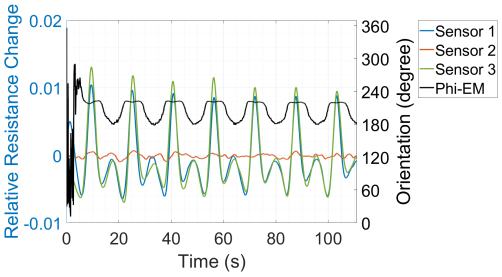

(b) Chamber 2

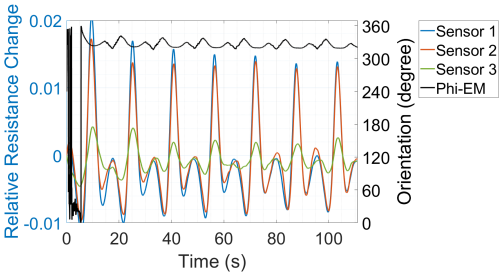

(c) Chamber 3

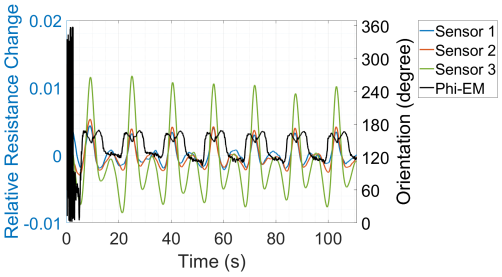

(d) Chamber 12

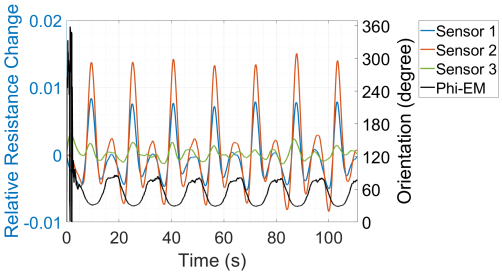

(e) Chamber 13

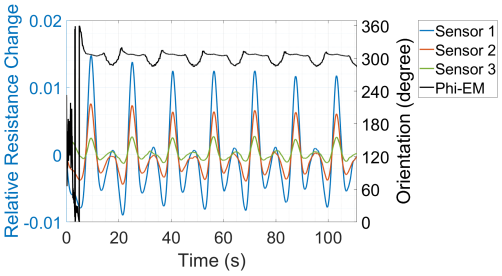

(f) Chamber 23

Figure C.3: Relative resistance change data for each chamber activation compared with orientation angle from the EM tracker (trial 1).

Appendix D

THE THIRD TRIAL RESULTS

D.1 Bending Angle

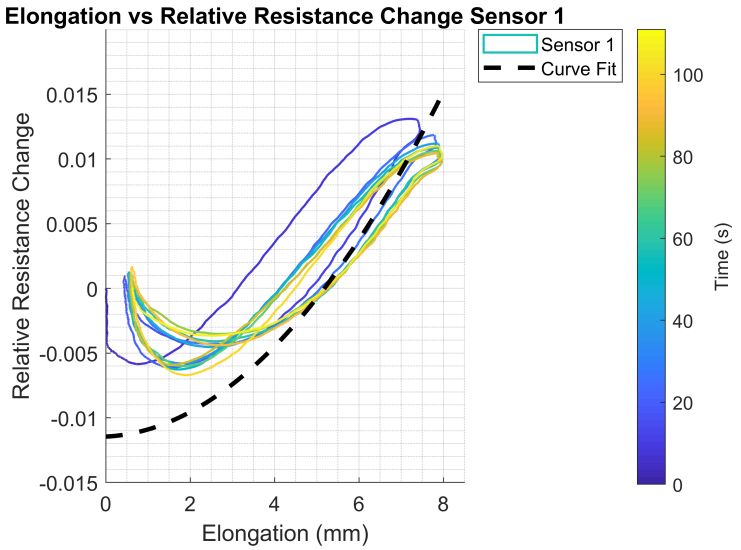

(a)

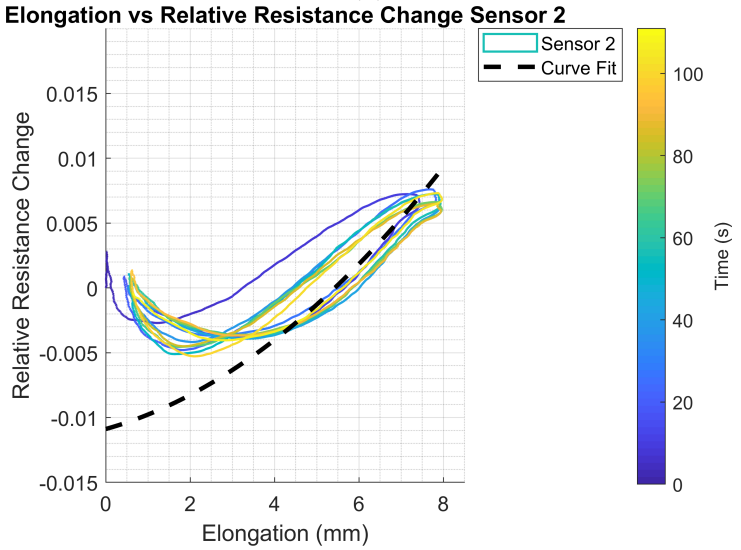

(b)

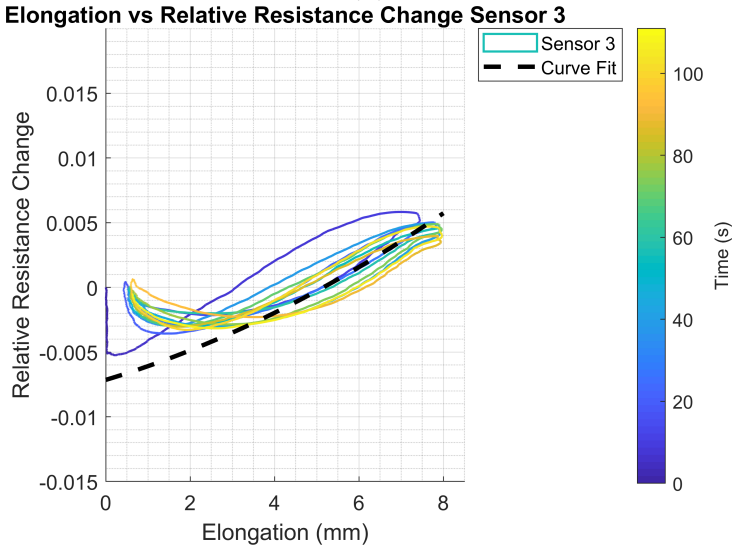

(c)

Figure D.1: Hysteresis curve with curve-fitted graph from trial 3.

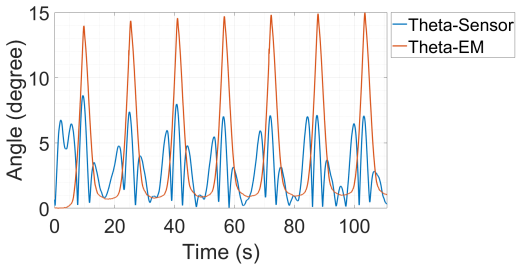

(a) Chamber 1

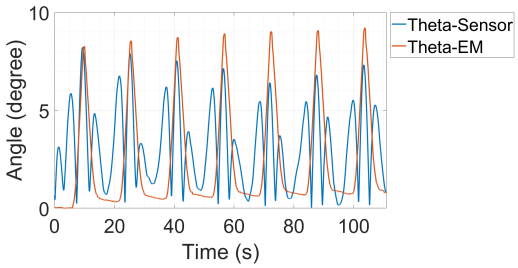

(b) Chamber 2

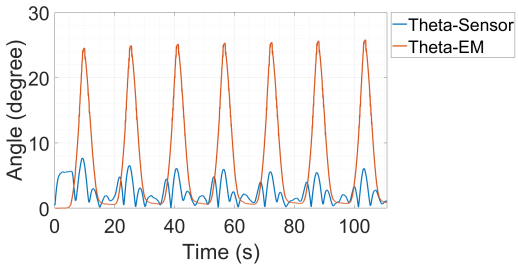

(c) Chamber 3

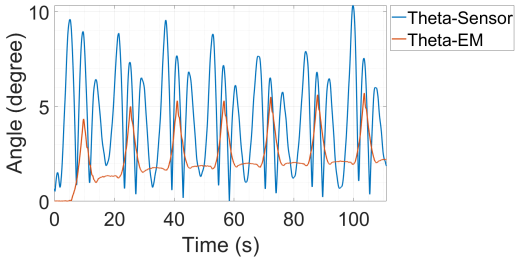

(d) Chamber 12

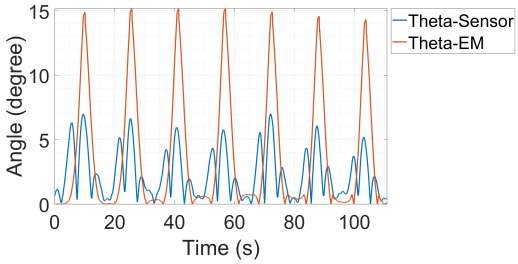

(e) Chamber 13

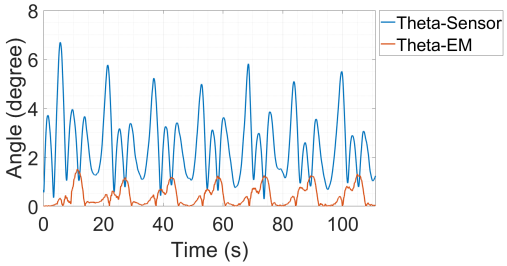

(f) Chamber 23

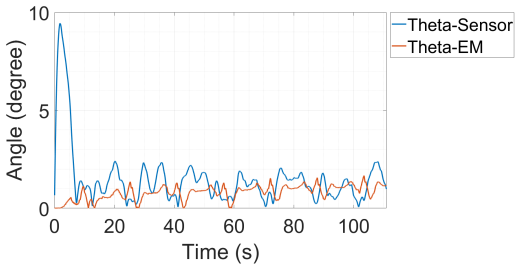

(g) Chamber 123

Figure D.2: Validation of bending angle from the 3D printed sensors with bending angle from the EM tracker (trial 3).

D.2 Orientation Angle

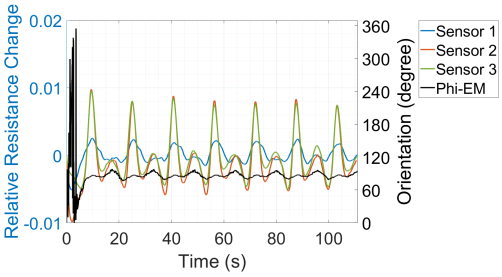

(a) Chamber 1

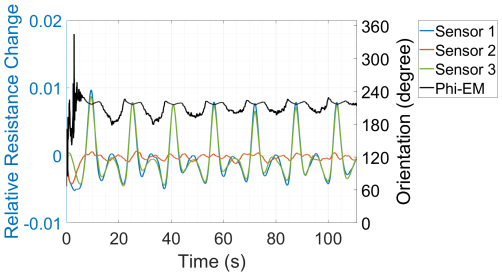

(b) Chamber 2

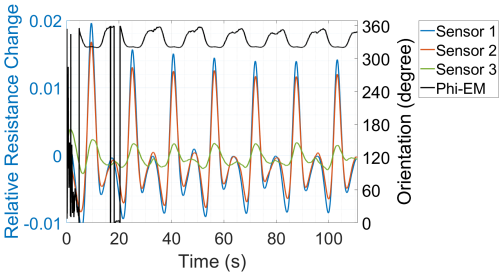

(c) Chamber 3

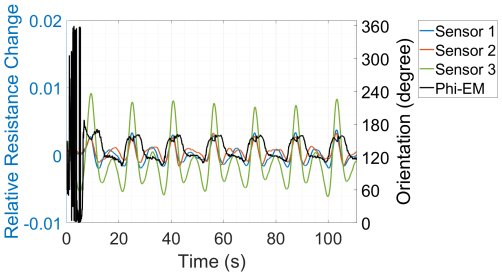

(d) Chamber 12

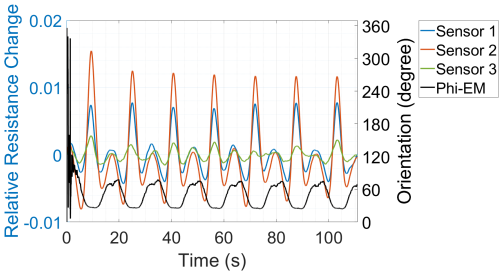

(e) Chamber 13

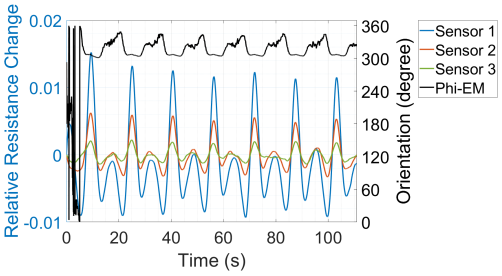

(f) Chamber 23

Figure D.3: Relative resistance change data for each chamber activation compared with orientation angle from the EM tracker (trial 3).